



8-2020

LAGRANGIAN BEDLOAD MOVEMENT PREDICTION USING THE VIRTUAL VELOCITY APPROACH

Theodoros Kyriakopoulos

University of Tennessee, Knoxville, tkyriako@vols.utk.edu

Follow this and additional works at: https://trace.tennessee.edu/utk_gradthes



Part of the [Environmental Engineering Commons](#)

Recommended Citation

Kyriakopoulos, Theodoros, "LAGRANGIAN BEDLOAD MOVEMENT PREDICTION USING THE VIRTUAL VELOCITY APPROACH. " Master's Thesis, University of Tennessee, 2020.
https://trace.tennessee.edu/utk_gradthes/6264

This Thesis is brought to you for free and open access by the Graduate School at TRACE: Tennessee Research and Creative Exchange. It has been accepted for inclusion in Masters Theses by an authorized administrator of TRACE: Tennessee Research and Creative Exchange. For more information, please contact trace@utk.edu.

To the Graduate Council:

I am submitting herewith a thesis written by Theodoros Kyriakopoulos entitled "LAGRANGIAN BEDLOAD MOVEMENT PREDICTION USING THE VIRTUAL VELOCITY APPROACH." I have examined the final electronic copy of this thesis for form and content and recommend that it be accepted in partial fulfillment of the requirements for the degree of Master of Science, with a major in Environmental Engineering.

Dr. John Schwartz, Major Professor

We have read this thesis and recommend its acceptance:

Dr. James Coder and Dr. Jon Hathaway

Accepted for the Council:

Dixie L. Thompson

Vice Provost and Dean of the Graduate School

(Original signatures are on file with official student records.)

**LAGRANGIAN BEDLOAD MOVEMENT
PREDICTION USING THE VIRTUAL VELOCITY
APPROACH**

A Thesis Presented for the
Master of Science
Degree
The University of Tennessee, Knoxville

Theodoros Kyriakopoulos
August 2020

ACKNOWLEDGMENTS

I would first like to thank my family for supporting me from the start of my studies and gave me the chance to be where I am right now. I would like to express my gratitude to my advisor, Dr. John S. Schwartz for his mentorship and for sharing his expertise relating to the subject of my research. I would also like to thank my co-worker and friend Micah Wyssmann for his insightful ideas and valuable discussions during our collaboration for my thesis experiments and analysis. I want to thank Dr. James Coder and Dr. Jon Hathaway for serving on my committee and providing critical comments that helped improve the quality of my thesis. I would like to thank Andrew Tsai for his assistance during the experiments for this study. I also want to thank Dr. Thanos Papanicolaou and Douglas Knapp for the development of an experimental methodology that was adopted for the experiments of this study. Finally, I would like to acknowledge the Chancellor's Top Off Fellowship from the University of Tennessee that supported me financially throughout the pursuit of my degree.

ABSTRACT

The advances in particle tracking codes in the recent years has made possible to track the intermittent movement of a large number of sediment particles with precision and in an automated way. The present study used this technique to study the velocity of the particle while it is in motion, the length it travels once it gets mobilized until it deposits, and the time it rests once deposited until it gets mobilized again. New modeling equations were developed to predict these quantities for a wide range of flow conditions and sediment sizes. These equations were combined to predict the virtual velocity of sediment, which is an equivalent velocity that accounts for both the moving and the resting time periods.

This laboratory experimental study involved controlled flume tests where spherical particles were transported by the flow on top of a well-packed bed. The moving particles were gravel-size and their diameter ranges from 0.43 to 1.35 times the diameter of the bed particles. The sediment transport stage ranged from incipient motion conditions (where particles were in motion only 2% of the total time), all the way to general motion where the particles almost never rested. A total of 25 experimental conditions were tested using a combination of 7 different flows and 5 different particle diameters. The particle trajectory was monitored by a camera and tracked using an open source particle tracking code. For each condition the mean resting time, displacement length and displacement time were calculated. On average, 120 data points were collected for each condition to get an accurate estimate of the average values of these three components. Equations were developed to predict these components as a function of the flow condition and sediment size. These equations were then combined to predict the virtual velocity of the sediment particles. The results of this study give insight to the physics that dominates the particle transport. Further research is needed to expand the use of these equations for natural sediment beds so they can better predict sediment transport rates in rivers.

TABLE OF CONTENTS

1	Introduction.....	1
2	Literature Review.....	4
2.1	Definition of Displacement Velocity and Virtual Velocity of Bedload .	4
2.2	Equations Developed in the Literature	6
2.2.1	Resting Time	6
2.2.2	Displacement Length	6
2.2.3	Displacement Time	8
2.2.4	Entrainment Rate	9
2.2.5	Displacement Velocity.....	9
2.2.6	Virtual Velocity	10
2.2.7	Bedload Discharge Definitions Using Lagrangian Quantities.....	12
3	Materials and Methods.....	17
3.1	Dimensional Analysis	17
3.2	Description of the Experimental Setup	19
3.3	Design of the Experiments.....	22
3.4	Calculating Virtual Velocity Components.....	24
3.4.1	Pre-Processing.....	24
3.4.2	Particle Tracking.....	25
4	Results and Discussion	28
4.1	Flow Characteristics.....	28
4.2	Particle Transport Tests	30
4.3	Proportion and Persistence of Motion.....	31
4.4	Critical Shear Stress for Well-Packed Marble Beds	33
4.5	Virtual Velocity Components	36
4.5.1	Resting Time	36
4.5.2	Displacement Length	38
4.5.3	Displacement Velocity.....	38

4.5.4	Virtual Velocity	40
5	Conclusions and Recommendations	44
	References	46
	Appendices	51
A	Averaging Methods for Displacement Velocities	52
B	Statistics of Resting Times	55
	Vita	59

LIST OF FIGURES

Figure 2.1 An intermittent trajectory of a sediment particle and the definition of resting time, T_r , displacement time, T_d , displacement length, L , displacement velocity, U_{sd} , and virtual velocity, U_{sv}	5
Figure 3.1 Experimental setup for monitoring the trajectories of transported particles. ..	20
Figure 3.2 Hexagonal close packing arraignment of bed marbles (top). Different size marbles used for the particle transport tests (right).	21
Figure 3.3 Error in streamwise position due to error in perspective requiring correction using the vertical coordinate of the tracked particle. The two blue marbles on the left and the two the right have the same streamwise position.	25
Figure 3.4 Example of part of a single trajectory plotted to manually record the resting and the mobilization times and locations. Particle moves from right to left.	27
Figure 4.1 Mean flow profiles measured using a side looking 3D SonTek 10 MHz ADV. All flume experiments had a flow depth equal to 12 cm.	29
Figure 4.2 Comparison of the calculated u^* values measured from the ADV profiles, with the square root of g_{RS} and g_{HS} which are the lower and upper boundary respectively. A side wall corrected value of u^* that is calculated using the equations proposed by Cheng and Chua (2005) is plotted as well.	30
Figure 4.3 Proportion of motion as a function of τ^* for all different R_r values of this study.	32
Figure 4.4 Persistence of motion is investigated by plotting a) the number of intermittent trajectories per unit time, and b) the mean displacement length, as a function of the proportion of motion. Proportion of motion is defined in Eq.(38).	32
Figure 4.5 Critical shear stress as function of relative roughness collapses with the m power equal to 1.33.	35
Figure 4.6 Dimensionless resting time as a function of a) τ^* , and b) $\tau^* R_r^{1.33}$	37

Figure 4.7 Dimensionless displacement length as a function of a) τ^* , and b) $\tau^* R_f^{1.33}$	39
Figure 4.8 Plot of the study data with the computed lines from Eq.(12) by Cheng and Emadzadeh (2014) using the values they proposed for their constants in Eq.(12). .	40
Figure 4.9 Virtual velocity data plotted along with the computed virtual velocity lines for different R_f values.	42
Figure 4.10 Comparison of the calculated and the measured virtual velocities.	43
Figure A.1 Differences in averaging method for displacement velocity.	53
Figure A.2 Non-linear relationship between displacement length and displacement time for the smaller displacements for the experiment with R_f equal to 0.84 and τ^* equal to 0.0152.....	54
Figure B.1 Normalized probability density functions of resting times corresponding to different transport stages for R_f equal to 0.84.	55
Figure B.2 Shape parameter for Weibull and Gamma distributions as a function of dimensionless resting time.	58
Figure A.1 Differences in averaging method for displacement velocity.	53
Figure A.2 Non-linear relationship between displacement length and displacement time for the smaller displacements for the experiment with R_f equal to 0.84 and τ^* equal to 0.0152.....	54

1 INTRODUCTION

Bedload transport (sediment particles that move near the bed either by rolling or by saltating) is one of the most important drivers of geomorphological changes in rivers. Improving the accuracy of the estimations of bedload transport rates is needed by water resources and environmental engineers, geomorphologists, ecologists and land-use planners. The prediction of bedload transport rates has been a challenging problem, and efforts to solve this problem go back to the work of Einstein (1950) and Meyer-Peter and Müller (1948). More empirical studies published in the years that followed tried to come up with equations to predict sediment bedload transport rates. An exhaustive list of the conventional sediment transport formulas considering Eulerian methods have been compiled by García (2008). Typically, the conventional equations cannot predict the sediment discharge very efficiently for low-flow conditions. Yet, the low-flow conditions contribute significantly to the total sediment load, due to the higher frequency of their events compared to higher flow events.

During lower flow conditions, when the mean flow is not capable of moving the sediment, the motion of the sediment particles is intermittent due to turbulence fluctuations in the hydrodynamic forces acting on the sediment particles. During these conditions, the sediment particles experience partial transport, i.e. not all the sediment particles in the bed are mobile. Haschenburger and Wilcock (2003) mention that 25-50% of the channel width experienced partial transport during the 2 year recurrence interval flood. Mao et al. (2017) indicate that partial transport condition could represent more than 70% of the total bed material transported during low-magnitude floods, and up to 40% for near-bankfull events.

A Lagrangian approach has potential to better predict partial bedload transport. A Lagrangian approach applies grain-scale physics and has led research in recent years to developing Lagrangian bedload transport formulas (Ballio et al. 2018; Haschenburger and Church 1998; Mao et al. 2017). Some of these studies use the virtual velocity of the

sediments to predict bedload transport. Virtual velocity is defined as the velocity that the sediment should move to travel the same total distance as it travels in intermittent states of moving and resting. Thus, the virtual velocity is calculated as the displacement length of the particles divided by the sum of the resting time and the displacement time. The concept of applying a Lagrangian virtual velocity formula would improve estimates of bedload transport flux.

Even though the virtual velocity has received increasingly more attention in multiple field and laboratory studies (Haschenburger and Church 1998; Klösch and Habersack 2018; Mao et al. 2017; Milan 2013; Papanicolaou et al. 2002a; Parsons et al. 2018), the development of a single formula to accurately predict virtual velocity of sediment particles is still an open question. Different studies not only provide equations that their predictions of virtual velocity vary significantly in magnitude, but also the relationship of the parameters used in these studies with virtual velocity are not fundamentally understood. This lack of fundamental understanding can be observed by looking at the sensitivity of the equations to the parameters, which can have opposite signs depending on the study (Mao et al. 2017; Milan 2013). In order to gain insight to the relationship of each parameter to virtual velocity, controlled laboratory flume experiments that examine a wide range of values for each parameter are needed. The advantage of controlled laboratory experiments is that the uncertainties relating to sediment particle size, bed roughness and flow stage are eliminated, and the particle trajectories can be monitored with high accuracy.

The major findings and result of this study include the development of equations to predict the subcomponents of virtual velocity (displacement length, resting time, and displacement time). These equations can then be used to predict the virtual velocity of different size fractions moving on top of a well-packed bed. This study focuses only on rolling motion of particles and does not consider saltation. The hypothesis of this research is that the physics that dominates the rolling motion and the bedload transport rates in moderate slope gravel-bed rivers can be accounted by two dimensionless parameters, the

dimensionless bed shear stress parameter and the relative roughness defined as the ratio of the moving particle diameter to the mean bed particle diameter.

2 LITERATURE REVIEW

2.1 Definition of Displacement Velocity and Virtual Velocity of Bedload

Movement of sediment bedload particles in open channel streams is intermittent due to the stochastic nature of turbulence and bed resistance. The mean flow generally is not capable of moving the particles, but when a turbulent fluctuation in the flow velocity generates a momentum impulse on a resting particle that exceeds a critical value, it will mobilize the resting particle (Celik et al. 2013). The particle will travel until the flow forces are not capable to keep it in motion and then the particle deposits again on the bed. This intermittent movement is presented in Figure 2.1, where the definition of resting time, T_r , displacement time, T_d , and displacement length, L are also shown.

The values for L , T_d , and T_r vary in each intermittent trajectory (which is defined as the trajectory starting from a mobilization event until the end of resting after deposition, i.e., until the next mobilization event). However, for a sufficiently long flow event the mean values of these components can be used to predict the long term distance that a particle would travel during that flow event (Ballio et al. 2018). Virtual velocity U_{sv} is an equivalent velocity that can be used to estimate how far the sediment particle would travel in a given time and accounts for both resting and displacement periods

$$U_{sv} = \frac{\bar{L}}{\bar{T}_d + \bar{T}_r} \quad (1)$$

The mean displacement velocity can also be calculated using the mean values for displacement and displacement time

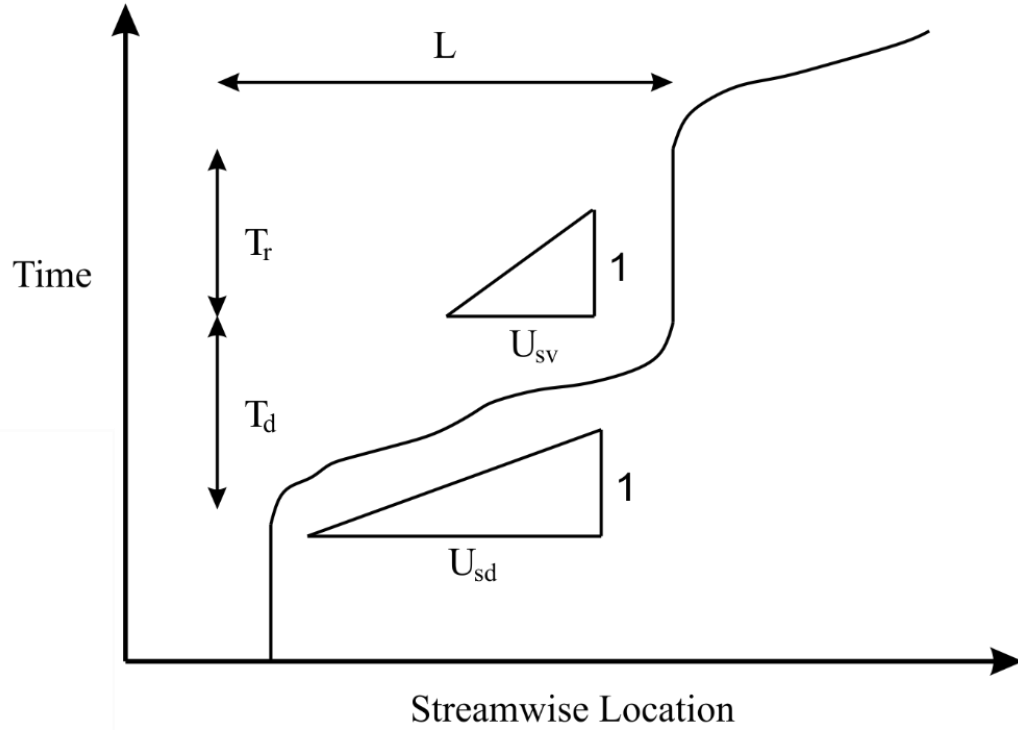


Figure 2.1 An intermittent trajectory of a sediment particle and the definition of resting time, T_r , displacement time, T_d , displacement length, L , displacement velocity, U_{sd} , and virtual velocity, U_{sv} .

$$U_{sd} = \frac{\bar{L}}{\overline{T_d}} \quad (2)$$

Here it is important to note that the value of Eq.(22) is different than the mean of the displacement velocities for each intermittent trajectory, something that has been pointed out in the literature (Ballio et al. 2018; Fathel et al. 2015). In Appendix A, the data of the present study further supports this claim. Thus, Eq.(1) through appropriate averaging predicts long-term displacement of particles.

2.2 Equations Developed in the Literature

2.2.1 *Resting Time*

Currently, the author has not found any equation developed in the literature to predict the resting times of sediment particles. There are, however, some studies that present resting time data (Niño and García 1998; Papanicolaou et al. 2002a; Wu and Yang 2004).

2.2.2 *Displacement Length*

Lajeunesse et al. (2010), through experimentation, developed an equation for the displacement length for both saltating and rolling natural sand particles. The equation is presented below:

$$\frac{\bar{L}}{d} = (70 \pm 2) \frac{u^* - u_c^*}{V_s} \quad (3)$$

in which the shear velocity, u^* , and fall velocity of particle, V_s , are calculated with the equations presented below:

$$\tau = \rho_w u^{*2} \quad (4)$$

$$V_s = \sqrt{\left(\frac{\rho_s}{\rho_w} - 1\right) dg} \quad (5)$$

where d is the particle diameter, τ is the bed shear stress, u_c^* is the critical value of shear velocity u^* to cause sediment motion, ρ_s and ρ_w are the particle and water densities respectively, and g is the acceleration of gravity.

Hunt and Papanicolaou (2003) developed the theoretical formula below based on a probabilistic treatment of the entrainment and deposition processes, focusing on the interaction of turbulent eddies with sediment particles. The equation is as follows:

$$L = C \frac{\tau}{d} \log\left(\frac{a\tau}{d_{50}} - \frac{d}{bd_{50}}\right) \quad (6)$$

where C , a and b are constants that require calibration. The constant C has units of (m s²/kg), and the constant a has units of (s²/kg).

Wong et al. (2007), proposed an equation for the mean displacement length of uniform gravel as a function of excess shear stress, and it is presented below:

$$\frac{\bar{L}}{d} = 53.2(\tau^* - \tau_c^*)^{-0.35} \quad (7)$$

This equation was empirically derived from measurements of bedload transport rate and total entrainment rates. The negative power of τ^* was explained with the increase in bed elevation fluctuations with an increasing τ^* .

Two relationships that were found in the literature incorporate the relative roughness term, but instead of predicting actual magnitude for the displacement length they predict relative displacement in respect to the displacement of the median particle size, with diameter equal to d_{50} . Church and Hassan (1992) proposed the equation below:

$$\log\left(\frac{\bar{L}_i}{\bar{L}_{50}}\right) = 0.232 + 1.35 \log\left(1 - \log\left(\frac{d_i}{d_{50}}\right)\right) \quad (8)$$

where \bar{L}_{50} is the displacement of the median particle size fraction and d_{50} is its diameter. The i subscript denotes the i -th size fraction (i.e., the i is the percentage of the total number of grains that have a diameter smaller than the diameter of the i -th size fraction). Vázquez-Tarrío et al. (2019) compiled data from 33 studies and fitted a formula similar to Eq.(8) which is presented below:

$$\log\left(\frac{\bar{L}_i}{\bar{L}_{50}}\right) = -0.26 \frac{d}{d_{50}} + 0.26 \quad (9)$$

2.2.3 Displacement Time

Lajeunesse et al. (2010) also developed an equation for the displacement time normalized using a falling velocity timescale that is equal to the diameter of the particle divided by the terminal fall velocity:

$$\frac{\bar{T}_d}{\sqrt{\frac{d}{\left(\frac{\rho_s}{\rho_w} - 1\right)g}}} = 10.6 \pm 0.7 \quad (10)$$

2.2.4 Entrainment Rate

The entrainment rate is the number of particles entrained per unit area of the channel bed per unit time. Wong et al. (2007) proposed a dimensionless equation for the entrainment rate, E , of uniform gravel as function of the excess shear stress $\tau^* - \tau_c^*$, where τ_c^* is the critical value of τ^* to cause sediment motion. The equation is as follows:

$$\frac{E}{\sqrt{\left(\frac{\rho_s}{\rho_w} - 1\right) g d_{50}}} = 0.05(\tau^* - \tau_c^*)^{1.85} \quad (11)$$

2.2.5 Displacement Velocity

Cheng and Emadzadeh (2014) proposed the semi-empirical formula of Eq.(12) for the displacement velocity. The first term accounts for the forces of the flow that keep the particle in motion and the second term is related to the friction due to collisions with the bed that resist the motion of the particle.

$$U_{sd}^* = c_1 \sqrt{\tau^*} - c_2 \left(\frac{1}{R_r}\right)^n \quad (12)$$

Where c_1 and c_2 are experimental constants, τ^* is the dimensionless bed shear stress, and R_r is the relative roughness defined below:

$$\tau^* = \frac{u^*}{\left(\frac{\rho_s}{\rho_w} - 1\right) g d} \quad (13)$$

$$R_r = \frac{d}{d_{50}} \quad (14)$$

The dimensionless displacement velocity is defined as follows:

$$U_{sd}^* = \frac{U_{sd}}{\sqrt{\left(\frac{\rho_s}{\rho_w} - 1\right)gd}} \quad (15)$$

2.2.6 Virtual Velocity

Mao et al. (2017) developed an equation to predict the virtual velocity of each size fraction of natural sediments as a function of τ^* and R_r :

$$\log\left(\frac{U_{sv}}{\sqrt{gd}}\right) = -a - b R_r + c \tau^* \quad (16)$$

where the value for the experimental constant a is equal to 4.56, the value of the constant b ranges from 0.24 to 0.42 and the value of the constant c ranges from 35.39 to 36.55. The range of the coefficients b and c is due to that Mao et al. (2017) fitted the coefficients for different rivers and reported the values for each one separately. A similar equation was also proposed in other studies (Ferguson et al. 2002; Ferguson and Wathen 1998).

Other studies proposed relationships using an excess shear stress term. Wong et al. (2007) proposed an excess shear stress relationship for the virtual velocity of uniform gravel as a function of the excess shear stress

$$\frac{U_{sv}}{\sqrt{\left(\frac{\rho_s}{\rho_w} - 1\right)gd}} = 1.67(\tau^* - \tau_c^*)^{0.90} \quad (17)$$

Klösch and Habersack (2018) also proposed non-linear equations using excess shear stress terms. One equation they proposed is based on the consideration that U_{sd} is linearly correlated with $\sqrt{\tau^*} - \sqrt{\tau_c^*}$ and particle activity is linearly correlated with $\tau^* - \tau_c^*$. This equation is as follows:

$$U_{sv} = a(\tau^* - \tau_c^*)(\sqrt{\tau^*} - \sqrt{\tau_c^*}) \quad (18)$$

where a is a constant. A second type of formula they proposed, used a power law of excess shear stress. The second type of equation is as follows:

$$U_{sv} = a(\tau^* - \tau_c^*)^b \quad (19)$$

where a and b are constants. They investigated a specific value of b equal to $3/2$, based on the Meyer-Peter and Müller (1948) formula for bedload sediment discharge and is dependent on the $(\tau^* - \tau_c^*)^{3/2}$ term. It should be noted here that the virtual velocity in Eq.(18) and Eq.(19) is not dimensionless, and the constant a has dimensions of velocity.

The previously presented equations of virtual velocity show that an increase in dimensionless bed shear stress or a decrease in relative roughness will result in an increase for the predicted virtual velocity value. Milan (2013) by using data from a natural river with multiple size fractions, proposed the equations below in which an increase in dimensionless bed shear stress or a decrease in relative roughness will result in a decrease instead of an increase for the predicted virtual velocity value:

$$\frac{U_{sv}}{\sqrt{gd}} = 94.818 R_r^{2.021} \quad (20)$$

$$\frac{U_{sv}}{\sqrt{gd}} = 0.0456 \tau^{*-2.1326} \quad (21)$$

This discrepancy in the equations from literature indicate the need to develop a more reliable equation for the prediction of the virtual velocity, or identify the transport domain equation can more accurately predict bedload transport flux.

Parsons et al. (2018) compiled data from literature and along with their flume experiments and suggest a power law relationship to predict virtual velocity for a very wide range of τ^* values ranging from 0.02 to 0.90. The equation is as follows:

$$U_{sv} = a \tau^{*b} \quad (22)$$

where a is equal to 58209 m/h (meters per hour) and the constant b is equal to 3.4434. While they present the strength of this relationship as a hypothesis for a holistic approach to sediment transport, they also point out that there is lack of data in the finer size range ($d < 4$ mm) to validate the use of this equation for all sediment sizes.

2.2.7 Bedload Discharge Definitions Using Lagrangian Quantities

There are three different definitions found in the literature that use the Lagrangian quantities to calculate Eulerian sediment discharge fluxes. They use either (i) a mean displacement length and an entrainment rate per unit area and unit time, (ii) a displacement velocity and an estimation of the number of particles that are in motion, or (iii) a virtual velocity.

The first definition was introduced by Einstein (1950) and still attracts attention from the community (Fraccarollo and Hassan 2019). This definition focuses on the displacement length of bedload particles. The equations of this definition are presented below:

$$\tilde{q}_s = \tilde{E} \tilde{L} \tilde{V}_p \quad (23)$$

$$\tilde{q}_s = \frac{q_s}{\sqrt{g \left(\frac{\rho_s}{\rho_w} - 1 \right) d^3}} \quad (24)$$

$$\tilde{E} = E \sqrt{\frac{d^5}{g \left(\frac{\rho_s}{\rho_w} - 1 \right)}} \quad (25)$$

$$\tilde{V}_p = \frac{V_p}{d^3} \quad (26)$$

where q_s is the volumetric sediment transport rate per unit of width, \tilde{q}_s is the dimensionless volumetric sediment transport rate per unit of width, \tilde{E} is the dimensionless entrainment rate (number of particles entrained per unit surface area per unit time) of the particles, \tilde{L} is the dimensionless mean displacement length and \tilde{V}_p is the dimensionless representative particle volume.

The second definition, as used by Wu and Yang (2004) takes the form below using displacement velocity and an estimate of the number of particles that are in motion

$$q_{bi} = \frac{m_i F_i Y_i}{D_i^2} P_{M,i} \frac{L_i}{T_{d,i}} = \frac{m_i F_i Y_i}{D_i^2} P_{M,i} U_{sd,i} \quad (27)$$

$$\frac{F_i Y_i}{D_i^2} = N_i \quad (28)$$

where N_i is the number of particles of the i -th size fraction that are able to be mobilized, F_i is the proportion of the i -th size fraction in the surface grain size distribution, D_i is the diameter of the i -th size fraction, and Y_i is the fractional mobility (i.e., the percentage of the grains of this size fraction that can actually move during the transport event), m_i is the representative mass of each grain in this size fraction, $P_{M,i}$ is the probability that the particle is in the moving state, L_i is the mean distance this particle moves in each intermittent trajectory, and $T_{d,i}$ is the mean time spent in motion during that intermittent trajectory. When a fraction experiences full transport conditions, a correction term is introduced to account for more than one layer of mobilized particles per size fraction and Eq.(27) is modified as follows:

$$q_{bi} = \left(\frac{m_i F_i Y_i}{D_i^2} P_{M,i} U_{sd,i} \right) \Delta_i Y_i^{1.8} \quad (29)$$

where Δ_i is a correction parameter.

A third definition developed by Haschenburger and Church (1998) that uses the virtual velocity for predicting the sediment discharge, is the following:

$$G_b = w_s (1 - p) \rho_s d_s U_{sv} \quad (30)$$

where G_b is the sediment discharge in mass per unit time, d_s is the active layer depth, w_s is the active width of the streambed, p is the fractional porosity of the streambed and ρ_s is the density of the sediment. The formula of Haschenburger and Church (1998) cannot account for the different fractions that are in motion. This multi-fraction transport can be accounted by the framework of Wilcock and McArdeell (1997) as shown by Mao et al. (2017) in Eq.(31) below. In Eq.(31), q_i is the unit mass fractional transport rate of the sediments of the i -th size fraction, $U_{sv,i}$ is the virtual velocity of sediments of the i -th size fraction and M_i is the mass of sediments of the i -th size fraction entrained from a certain surface area over a certain time

$$q_i = \frac{m_i F_i Y_i}{D_i^2} U_{sv,i} \quad (31)$$

Eq.(31) refers to partial transport conditions. For full transport conditions, where grains from more than one layer get mobilized, Eq.(31) takes the form of

$$q_i = \frac{m_i F_i}{D_i^3} d_s U_{sv,i} \quad (32)$$

Mao et al. (2017) proposed an equation for the active layer depth, d_s and the partial transport as function of the dimensionless shear stress. The equation is as follows:

$$d_s = a \tau^{*b} \quad (33)$$

$$Y = 2.232 + 0.475 \log(\tau^*) \quad (34)$$

where the value of the constant a ranges from 2.897 to 3.578 and the value of the constant b ranges from 0.891 to 0.919. The values are from fitting the equations to data from natural rivers. Due to difficulties to obtain experimental values for each different size fraction in natural rivers these equations do not account for the effects of R_r . Wong et al. (2007) used measurements of bed elevation fluctuation to estimate the active layer depth for uniform gravel as function of the excess shear stress

$$\frac{s_y}{d_{50}} = 3.09(\tau^* - \tau_c^*)^{0.56} \quad (35)$$

$$\frac{d_s}{d_{50}} = 1.62s_y \quad (36)$$

where s_y is the standard deviation of bed elevation fluctuations.

It should be noted here that Eq.(27) and Eq.(31) are equivalent if Eq.(37) is considered

$$P_{M,i}U_{sd,i} = U_{sv,i} \quad (37)$$

The probability, $P_{M,i}$, in Eq.(37) is referred in the literature (Ballio et al. 2018) as proportion of motion and the definition in Eq.(38) can be derived directly using Eq.(1), Eq.(22) and Eq.(37)

$$P_{M,i} = \frac{\overline{T_d}}{\overline{T_d} + \overline{T_r}} \quad (38)$$

3 MATERIALS AND METHODS

3.1 Dimensional Analysis

The basis of this study's experimental design is from a dimensional analysis completed in Papanicolaou et al. (2002a). Papanicolaou et al. (2002a) used the Buckingham Pi Theorem and their analysis yielded six dimensionless terms that capture the physics of sediment transport by incorporating all relevant fluid, flow and sediment parameters in a functionality F of the form of Eq.(39) below:

$$U_{sv}^* = F \left[\frac{V_s}{\kappa u^*}, \frac{d}{d_{50}}, \frac{H}{d}, \frac{u^*}{\left(\frac{\rho_s}{\rho_w} - 1\right) g d}, \frac{u^* d}{v}, \left(\frac{\rho_s}{\rho_w} - 1\right) \right] \quad (39)$$

where the first term is the Rouse number equal to the fall velocity of the sediment particles, V_s , divided by the shear velocity, u^* , and the Von Karman constant, κ , the second term is the relative roughness R_r as defined in Eq.(14), the third term is the relative submergence in which H is the flow depth, the fourth term is the dimensionless bed shear stress where ρ_s is the density of the moving particle, ρ_w is the density of water and g is the acceleration of gravity, the fifth term is the particle Reynolds number where v is the kinematic viscosity of the sediment, and the last term is the dimensionless submerged weight of the sediment.

This study proposes a simplification of the functionality of Eq.(39) that is applicable in moderate slope gravel bed streams. Several assumptions were made in order to reduce the number of parameters presented in Eq.(39). First, the Rouse number can be dropped because this study is concerned about the rolling motion regime and not saltation. Also, by assuming that relative submergence is greater than 3 (i.e., flow depth is 3 times

greater than the particle diameter), which is typical in moderate slope gravel bed streams, the relative submergence does not affect the sediment transport rates (Bettess 1984). Furthermore, in gravel bed rivers the bed is typically hydrodynamically rough and the value of the critical shear stress (for incipient motion of sediment) becomes independent of the particle Reynolds number (Vanoni 2006). This is observed visually in the Shield's diagram (Shields 1936). The critical shear stress becomes constant when the particle Reynolds number becomes greater than 500. All tests in this study were in the hydrodynamically rough bed regime. It is assumed, therefore, that the particle Reynolds number can be dropped for simplification. Finally, since the dimensionless submerged weight of natural sediment in rivers is almost always a constant value (≈ 1.6), since sediment and water densities do not vary significantly, the dimensionless submerged weight parameter can be dropped too. After the assumptions above, the functionality in Eq.(39) becomes simpler and more practical. The new simplified functionalities that are proposed in this study for the virtual velocity subcomponents, can be used to calculate the virtual velocity from the definitions in Eq.(1) and Eq.(2). The simplified functionalities are presented below:

$$L^* = L^*(R_r, \tau^*) \quad (40)$$

$$T_r^* = T_r^*(R_r, \tau^*) \quad (41)$$

$$U_{sd}^* = U_{sd}^*(R_r, \tau^*) \quad (42)$$

where L^* is the dimensionless displacement length, T_r^* is the dimensionless resting time, and U_{sd}^* is the dimensionless displacement velocity.

3.2 Description of the Experimental Setup

Particle transport experiments were completed at the Hydraulics and Sedimentation Lab (HSL) at University of Tennessee, Knoxville. The flume of HSL has a width of 0.60 m and a length of 9.0 m (Figure 3.1). The slope of the flume is adjustable, and an inclinometer measures the flume slope with accuracy of 0.01 %. Uniform flow for all tests was achieved using a tailgate. The flume walls are made from acrylic and thus enable to monitor the particle movement from the side of the flume. The particle trajectories were monitored by a camera on a tripod from the side of the flume. The experimental methodology was based on the work of Knapp (2002). The bed was comprised by two layers of marbles with diameter of 18.5 mm. Hexagonal close packing (Figure 3.2) of the bed marbles was chosen, to achieve the lowest porosity possible (26 %), so the bed marbles would not mobilize during test (angle of repose is 90 degrees) and the bed roughness would be uniform. The moving particles were glass marbles with diameters of 8.0, 15.6, 18.5, 22.2 and 25.0 mm (Figure 3.2). The wide range of diameters was chosen to capture the effects of the roughness of the bed relative to the diameter of the moving particles, thus account for different size fractions found in gravel bed rivers. The ratio of the diameter of the moving particle to the diameter of the bed particles will be referred to in this thesis as relative roughness (R_r) as defined by Eq.(14). The flow depth, H was 12 cm for all tests. The ratio H/d is greater than 3 (for all particle diameters), thus the critical stress value is independent of H/d (Bettess 1984).



Figure 3.1 Experimental setup for monitoring the trajectories of transported particles.

For each particle diameter a wide range of flow conditions was examined to capture movement during both low and high transport (Table 3.1). The bulk flow was captured by a flowmeter and a detailed mean flow profile was captured using a side looking 3D SonTek 10 MHz Acoustic Doppler Velocimeter (ADV). The ADV was mounted on a traverse that moved it in the vertical direction using a motor. An electronic level was used to ensure the ADV was vertical with an angle error less than 0.1 degrees. The vertical position was able to be controlled with the motor with an error less than 0.003 mm. The velocity time series

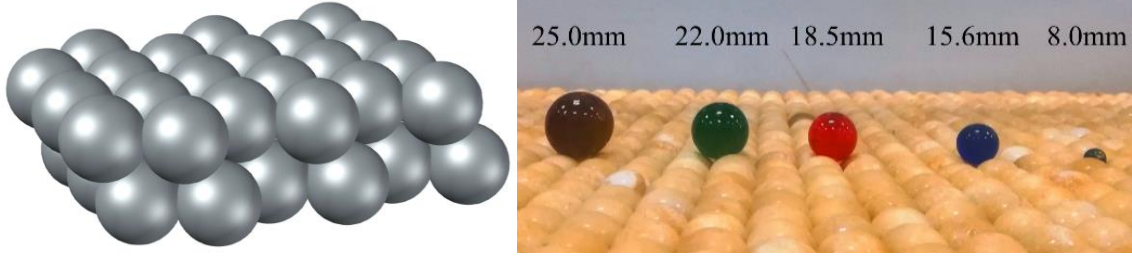


Figure 3.2 Hexagonal close packing arraignment of bed marbles (top). Different size marbles used for the particle transport tests (right).

for each different depth was 2 minutes long with data acquisition frequency of 25Hz which results in 3000 data points total, which is a widely accepted number for capturing mean flow profiles (García et al. 2005). The measurements were denser in the inner layer of the flow (lower 20% of flow depth). These measurements were used to calculate the bed shear stress (Clauser 1956) by fitting the profile to the log law (Kironoto and Graf 1995) by Eq.(43) below:

$$\frac{u}{u^*} = \frac{1}{\kappa} \ln \left(\frac{z + z_0}{k_s} \right) + B \quad (43)$$

where u is the streamwise velocity, κ is the Von Karman constant equal to 0.41, z is the coordinate with origin at the crest of the marbles, z_0 is the distance from the crest of the marbles to the zero velocity level, B is a constant and k_s is the characteristic hydrodynamic bed roughness height taken to be equal to the bed marble diameter (Papanicolaou et al. 2012).

3.3 Design of the Experiments

The downstream end of the flume test section of the experiments was located 1.5 m upstream of the tailgate and had a length of 2.3 m. The upstream end of the test section was located 5.2 m downstream of the headbox. This made sure that the flow would be fully developed, since 5.2 m is equal to 43 times the flow depth of 12 cm for these tests. A wide range of flow conditions was tested ranging from very low transport, lower than the widely accepted threshold for motion that is set to probability of entrainment equal to 2% (Papanicolaou et al. 2002b), to very high transport (approaching the general motion regime) for each size fraction.

The experiments were designed to capture the transport of isolated particles. For all tests it was made sure no particles were closer than 10 diameters with any other particle in the test section (at any time along their trajectories) to eliminate interaction. For the very low transport tests, particles were preplaced in the test section in approximately 0.1% packing density (ten particles in the test section that is 0.6 m wide and 2.3 m in length). For the intermediate transport conditions particles were preplaced, and when the test section started to get depleted from particles, particles were fed 1.0 m upstream of the test section. For the high transport tests, particles were just fed 1.0 m upstream of the test section. It was always made sure that particles rested at least one time before they enter the test section to eliminate errors related to initial velocity of the particle during feeding.

All the experimental conditions can be seen in the Table 3.1. For some tests, only the resting times were able to be obtained due to significant censoring of displacement lengths. Ballio et al. (2019) pointed out that censoring of displacement lengths is not negligible if the test section length is less than 10-15 times the mean values of displacement length. Censoring happens when a displacement takes place near the edge of the test section and part of the displacement is located outside of the test section. These displacements are not accounted in the calculation of the mean displacement length. The longer the displacement length, the higher the probability that part of it is located outside of the test

Table 3.1 Experimental conditions for the particle transport tests.

Flow #	$d_{50,b}$ (mm)	d_m (mm)	Rr (-)	S (-)	H (m)	u_* (m/s)	q (m ² /s)	U_b (m/s)	Fr (-)	$Re \times 10^4$ (-)	τ^* (-)
Flow 1	18.5	15.6	0.84	0.0024	0.12	0.0501	0.067	0.559	0.52	7.4	0.0106
	18.5	18.5	1.00								0.0089
	18.5	22.2	1.20								0.0074
	18.5	25.0	1.35								0.0066
Flow 2	18.5	15.6	0.84	0.0025	0.12	0.0526	0.069	0.576	0.53	7.6	0.0117
	18.5	18.5	1.00								0.0098
	18.5	22.2	1.20								0.0082
	18.5	25.0	1.35								0.0073
Flow 3	18.5	15.6	0.84	0.0026	0.12	0.0536	0.071	0.590	0.54	7.8	0.0121
	18.5	18.5	1.00								0.0102
	18.5	22.2	1.20								0.0085
	18.5	25.0	1.35								0.0076
Flow 4	18.5	8.0	0.43	0.0031	0.12	0.0568	0.074	0.620	0.57	8.2	0.0265
	18.5	15.6	0.84								0.0136
	18.5	18.5	1.00								0.0115
	18.5	22.2	1.20								0.0096
	18.5	25.0	1.35								0.0085
Flow 5	18.5	8.0	0.43	0.0036	0.12	0.0600	0.08	0.665	0.61	8.7	0.0296
	18.5	15.6	0.84								0.0152
	18.5	18.5	1.00								0.0128
Flow 6	18.5	8.0	0.43	0.0039	0.12	0.0633	0.084	0.699	0.64	9.2	0.0329
	18.5	15.6	0.84								0.0169
	18.5	18.5	1.00								0.0142
Flow 7	18.5	8.0	0.43	0.0048	0.12	0.0696	0.093	0.774	0.71	10.2	0.0398
	18.5	15.6	0.84								0.0204

section, i.e., the higher the probability that it gets censored. This results in shorter experimental mean values than the real mean values for the displacement length. The same applies for the resting times and the duration of the test. The duration for all tests was long enough (ranging from 2 to 8 hours long) to make sure the resting times were not censored.

3.4 Calculating Virtual Velocity Components

3.4.1 Pre-Processing

The videos of the moving particles were pre-processed before the tracking of the particle trajectories, using the Insight 4G software provided by TSI Inc. The pre-processing steps included:

- i. Creation of a background image by averaging all frames of the video
- ii. Subtracting this background image.
- iii. Subtracting a constant value of intensity to remove noise.
- iv. Smoothing the image using Gaussian smoothing with a window equal to the diameter of the moving particle.

To reduce processing time, the video frame rate was reduced to 7.5 frames per second (1/4 of the actual video framerate). This framerate was sufficient to capture resting times as low as 0.4 sec. There was only one test, the highest transport of the small 8 mm particle, where acceleration and transport velocity were so high that the full capacity of the cameras was used (60 frames per second).

3.4.2 Particle Tracking

Tracking of the particle trajectories was done using the open source MATLAB code, TracTrac (Heyman 2019). No background or noise removal was chosen in the settings using the TracTrac code since it was already done during pre-processing. The detector chosen was Difference of Gaussians (DoG) and the blob scale input chosen (i.e., the expected size of the detected particle in pixels) was the diameter of the moving particle. The intensity threshold was in 'Auto' and the sub-pixel method was chosen to be Gaussian. The motion model was unsteady with the default settings and no filtering of outliers was chosen. More information on the TracTrac code can be found in the work of Heyman (2019).

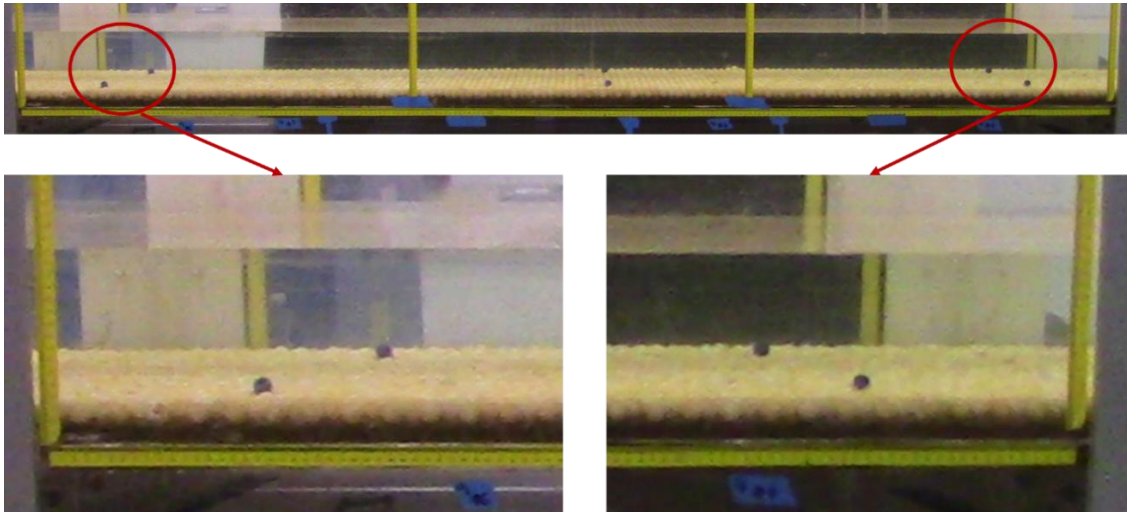


Figure 3.3 Error in streamwise position due to error in perspective requiring correction using the vertical coordinate of the tracked particle. The two blue marbles on the left and the two the right have the same streamwise position.

After tracking the particles, the data were filtered to exclude any marbles that were close to the walls, to eliminate side wall effects on the flow velocity field. Only the marbles that were more than one flow depth far away from the walls for the whole trajectory were considered for further analysis.

To measure the streamwise position of the particles, rulers were placed on the side of the flume to give a reference length. The perspective (Figure 3.3) in the videos was corrected using the vertical coordinate of the tracked particle. For each test, four control points were chosen using the marble layers of the bed that are perpendicular to the walls of the flume. Then two lines were fitted to these four control points that are the coordinates of the left and right edge of the test section. These two lines along with the vertical coordinate of the tracked particle were used to correct the streamwise position timeseries for the whole trajectory of every particle using its vertical coordinate timeseries.

To acquire the virtual velocity components, each trajectory (i.e., streamwise location timeseries) was plotted in MATLAB, and for each trajectory the time of the start and the end of resting, as well as the streamwise location were recorded manually. If there were more than 3 points with the same location this was identified as a resting event. Using this data the mean values of resting time, \bar{T}_r , displacement length, \bar{L} , and displacement time, \bar{T}_d , were calculated. Using these numbers, the displacement velocity U_{sd} and the virtual velocity U_{sv} were calculated using the Eq.(1) and the Eq.(22).

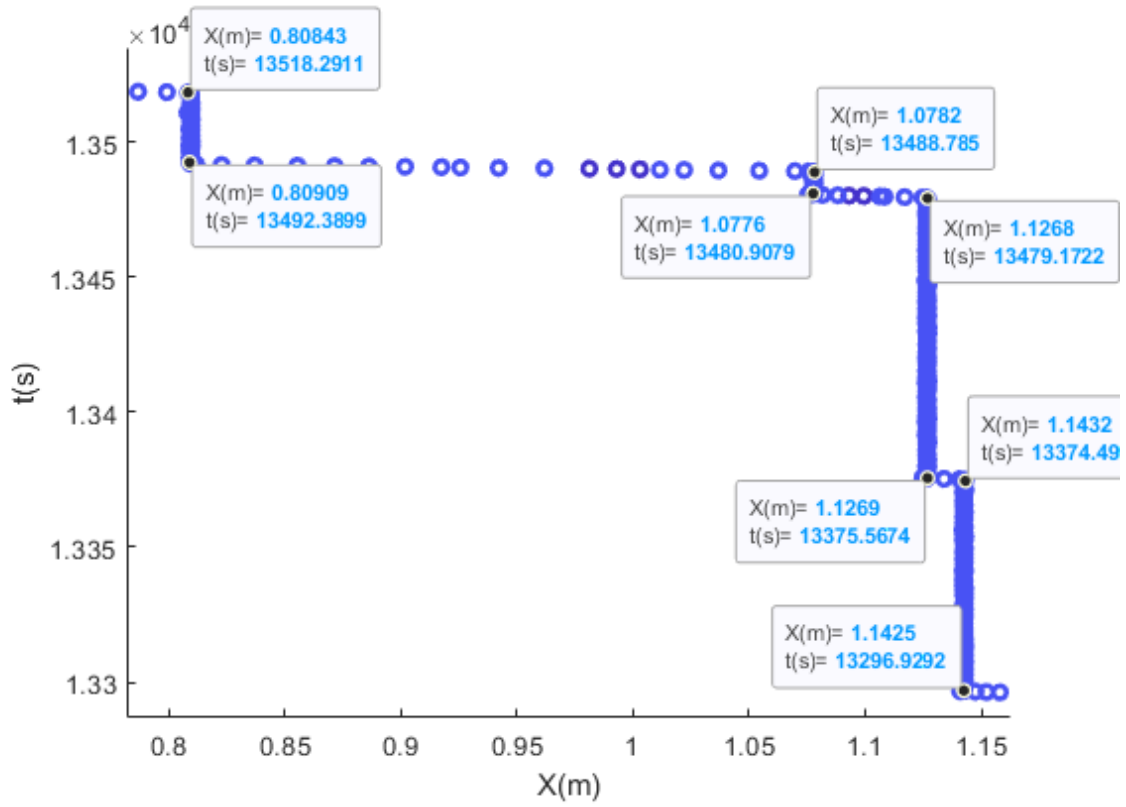


Figure 3.4 Example of part of a single trajectory plotted to manually record the resting and the mobilization times and locations. Particle moves from right to left.

4 RESULTS AND DISCUSSION

4.1 Flow Characteristics

To calculate the u^* for each flow condition, the mean flow profile was acquired using ADV measurements. The flow profiles can be seen in Figure 4.1. The values in the inner layer, which corresponds to the lower 20% of the flow depth, were used to calculate the u^* (Clauser 1956), by fitting the data to the log-law of Eq.(43). The calculated values of u^* for each different flow condition are the ones used in the analysis of this study.

To make sure the calculated u^* values are realistic, they are plotted in Figure 4.2 along with the square root of gHS and gRS that are the upper and lower boundaries for u^* respectively. The g is the acceleration of gravity, H is the flow depth, R is the hydraulic radius (area of flow divided by wetted perimeter) and S is the slope of the bed. The calculated u^* from the ADV profiles fall in between the upper and lower boundaries as expected.

A corrected value of the bed shear stress (Cheng and Chua 2005) is also plotted in Figure 4.2 that accounts for the different roughness between the bed and the flume walls. These values are very close to the calculated u^* values from the ADV profiles. The equations proposed by Cheng and Chua (2005) for the corrected bed shear stress are the following:

$$\frac{\tau}{\rho gHS} = 1 - 0.01a[\tanh \pi\beta - 0.5(\tanh \pi\beta)^2] \quad (44)$$

$$a = \exp \left[6.211 - 3.264 \log \left(\frac{B}{H} + 3 \right) \right] \quad (45)$$

$$\beta = 1 - 0.2 \log \left(\frac{k_{sb}}{k_{sw}} \right) \quad (46)$$

where H is the flow depth, S is the slope, B is the flume width, k_{sb} and k_{sw} are the characteristic hydrodynamic roughness of the bed and the flume wall respectively. The value of k_{sw} for smooth flume wall was proposed by Cheng and Chua (2005) to be 0.0015 mm.

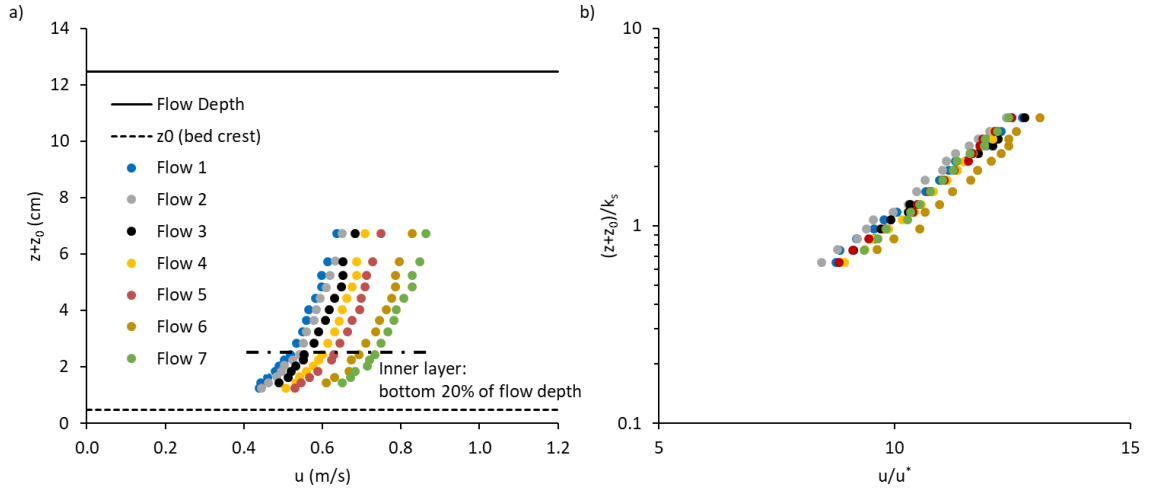


Figure 4.1 Mean flow profiles measured using a side looking 3D SonTek 10 MHz ADV. All flume experiments had a flow depth equal to 12 cm.

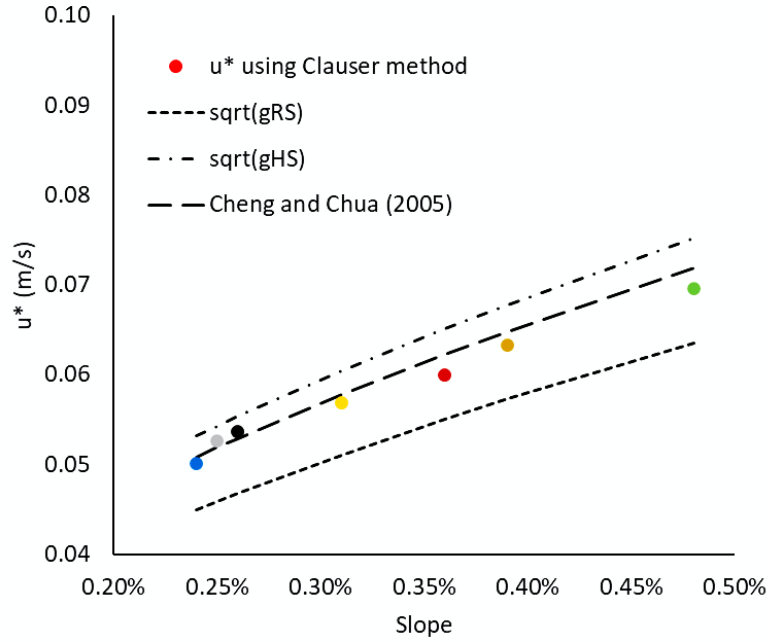


Figure 4.2 Comparison of the calculated u^* values measured from the ADV profiles, with the square root of gRS and gHS which are the lower and upper boundary respectively. A side wall corrected value of u^* that is calculated using the equations proposed by Cheng and Chua (2005) is plotted as well.

4.2 Particle Transport Tests

The results for the virtual velocity components were compiled and presented in Table 4.1. The empty entries in the table correspond to the tests where the displacement length was so long that was not experimentally feasible to capture it or the results would be significantly censored (Ballio et al. 2019) since the test section is only 2.3 m long. The resting times were able to be captured for all the tests since the test durations were long enough to make sure the results were not censored for any flow conditions.

Table 4.1 Results for virtual velocity and mean values of its components.

Flow #	u^* (m/s)	d (mm)	Rr (-)	τ^* (-)	L (m)	T_r (s)	T_d (s)	Usd (m/s)	Usv (m/s)
Flow 1	0.050	15.6	0.84	0.0106	0.049	661.5	1.7	0.029	7.4E-05
		18.5	1.00	0.0089	0.114	392.4	2.7	0.042	2.9E-04
		22.2	1.20	0.0074	0.136	237.1	2.9	0.047	5.7E-04
		25.0	1.35	0.0066	0.234	564.4	5.1	0.046	4.1E-04
Flow 2	0.053	15.6	0.84	0.0117	0.046	321.4	2.1	0.021	1.4E-04
		18.5	1.00	0.0098	0.086	302.8	2.3	0.038	2.8E-04
		22.2	1.20	0.0082	0.193	171.5	3.0	0.064	1.1E-03
		25.0	1.35	0.0073	0.291	394.4	5.9	0.049	7.3E-04
Flow 3	0.054	15.6	0.84	0.0121	0.060	133.4	1.8	0.033	4.5E-04
		18.5	1.00	0.0102	0.132	107.0	2.1	0.064	1.2E-03
		22.2	1.20	0.0085	0.260	84.9	3.3	0.080	3.0E-03
		25.0	1.35	0.0076	0.430	86.3	5.1	0.084	4.7E-03
Flow 4	0.057	8.0	0.43	0.0265	0.019	504.7	0.9	0.022	3.8E-05
		15.6	0.84	0.0136	0.077	49.5	1.6	0.048	1.5E-03
		18.5	1.00	0.0115	0.118	73.2	2.1	0.057	1.6E-03
		22.2	1.20	0.0096	-	30.4	-	-	-
		25.0	1.35	0.0085	-	35.7	-	-	-
Flow 5	0.060	8.0	0.43	0.0296	0.045	116.0	1.1	0.042	3.9E-04
		15.6	0.84	0.0152	0.145	15.6	1.8	0.079	8.3E-03
		18.5	1.00	0.0128	0.277	22.2	3.2	0.087	1.1E-02
Flow 6	0.063	8.0	0.43	0.0329	0.064	49.9	0.9	0.071	1.3E-03
		15.6	0.84	0.0169	0.222	4.5	2.4	0.094	3.2E-02
		18.5	1.00	0.0142	0.382	4.1	4.0	0.096	4.7E-02
Flow 7	0.070	8.0	0.43	0.0398	0.123	9.4	0.6	0.191	1.2E-02
		15.6	0.84	0.0204	-	1.6	-	-	-

4.3 Proportion and Persistence of Motion

Persistence of motion is discussed by Ballio et al. (2018) and the concept of the persistence of motion provides information that is hidden when discussing about the proportion of motion. Persistence of motion is the tendency of the particle to move less frequently but for longer distances. This means that two particles with the exact same proportion of motion, can have totally different persistence of motion. Proportion of motion is defined in Eq.(38) as the percentage of time that the particle is actually in motion, and the data from this study are presented in Figure 4.3.

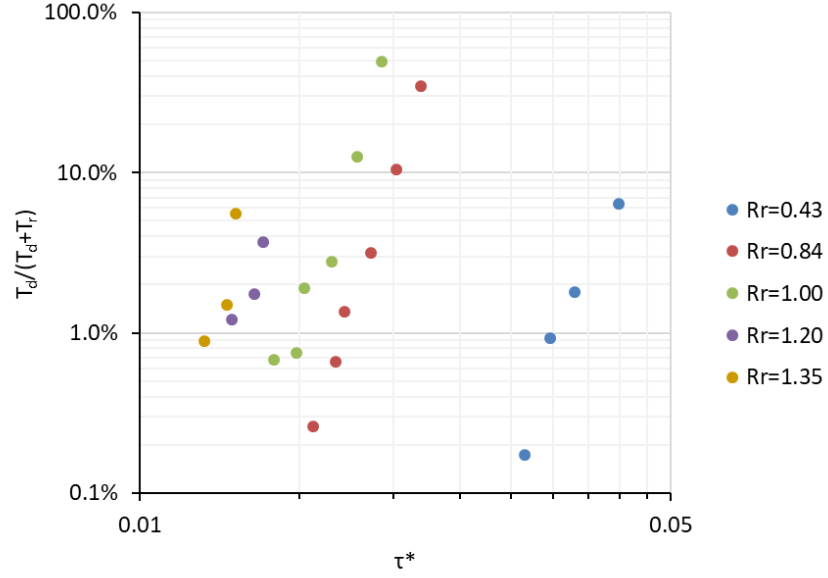


Figure 4.3 Proportion of motion as a function of τ^* for all different R_r values of this study.

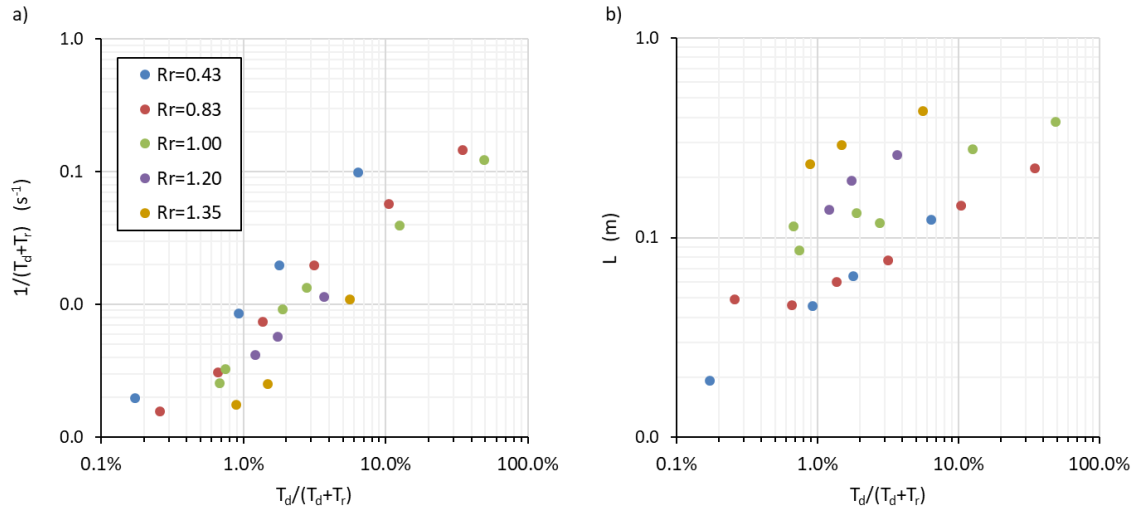


Figure 4.4 Persistence of motion is investigated by plotting a) the number of intermittent trajectories per unit time, and b) the mean displacement length, as a function of the proportion of motion. Proportion of motion is defined in Eq.(38).

The data from the present study in Figure 4.4 show a clear relationship between persistence of motion and R_r . For high R_r the mean displacement length increases and the rate of particle mobilization decreases for the same proportion of motion, which clearly shows that particles with higher R_r values move longer distances but less frequently than the particles with low R_r .

4.4 Critical Shear Stress for Well-Packed Marble Beds

Following the definition for the critical shear stress by Papanicolaou et al. (2002b), the critical shear stress was defined by using a stochastic definition of the 2% probability of entrainment, which can be thought as either that the 2% of all the particles of a certain size fraction are in motion or as the shear stress that keeps the particles in motion for 2% of the total time. Sediment transport models have used the concept of mobilization due to turbulent bursts (Papanicolaou et al. 2004) which assumes that particles get mobilized via coherent flow structures that have a consistent period of reoccurrence called the bursting period. For rough beds the bursting period, T_{burst} , scales with the average flow depth, H , and bulk flow velocity U_{bulk} as described by the equation below (Cantwell 1981):

$$T_{burst} = 6 \frac{H}{U_{bulk}} \quad (47)$$

An equation that is commonly used to calculate the critical shear stress $\tau_{c,i}^*$ for the i -th size fraction diameter is the following (Wu et al. 2000):

$$\tau_{c,i}^* = \tau_{c,50}^* R_r^{-m} \quad (48)$$

where $\tau_{c,50}^*$ is the dimensionless critical shear stress for of the median size fraction diameter, and m is a constant usually having a value of 0.6 for natural sediment. The physical meaning of the value of the power m is that if it is greater or lower than 1 determines if the critical shear stress is bigger for smaller or bigger particles respectively. The value of m equal to 1 is defined as equal mobility and has been used by some researchers as a hypothesis for predicting bedload discharge (Diplas 1987; Parker 1990).

Using the data from this study, two different approaches were undertaken based on the above in order to develop an equation to predict the critical shear stress for spheres resting on a well packed bed. One approach assumes that in a critical flow only the 2% of the bursts are capable to mobilize the particles, and by extrapolating from the resting time data (see equation developed in the next chapter) the shear stress that corresponds to resting time equal to 50 times the bursting period was calculated as the critical shear stress. The second approach used the proportion of motion (calculated by the measured data presented in the previous section), i.e., the percentage of the total time the particle spends in motion, and by extrapolation calculates the shear stress that predicts the proportion of motion to be equal to 2%. Again, the data from this study for resting time and for displacement time were used and the proportion of motion was calculated from Eq.(38). The analysis showed that for the well-packed bed of this study the value of m in Eq.(48) is equal to 1.33 and $\tau_{c,50}^*$ (which is the critical value for R_τ equal to 1) was calculated to be equal to 0.0109 (see Figure 4.5). This approach is an important difference compared to the value of 0.6, since 1.33 is higher than 1.

This analysis is useful to derive a parameter to predict the components of virtual velocity as function of τ^* and R_τ . The dimensionless shear stress normalized with critical shear stress yields a parameter that collapses the data from this study, as it will be shown in the next sections. This parameter is equal to:

$$\frac{\tau_i^*}{\tau_{c,i}^*} = \frac{\tau_i^*}{\tau_{c,50}^*} R_r^m = \frac{1}{0.0109} \tau_i^* R_r^{1.33} \quad (49)$$

The parameter $\tau_i^* R_r^{1.33}$ will be used to collapse the data of the virtual velocity components for different R_r values in the next sections. This parameter can be thought of as a corrected dimensionless critical shear stress that accounts for the hiding or exposure to the flow due to the relative size of the bed particles to the moving particles and the difference in bed resistance which is affected by the angle of repose.

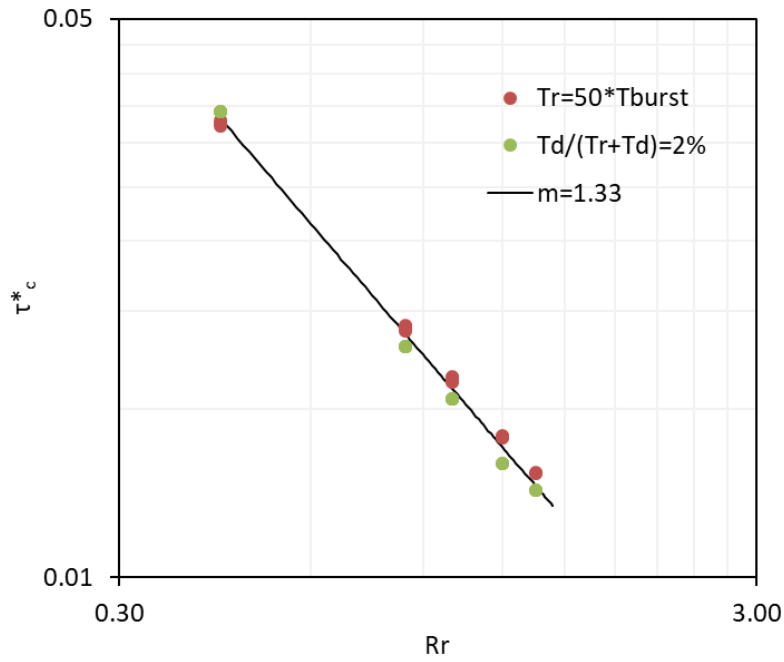


Figure 4.5 Critical shear stress as function of relative roughness collapses with the m power equal to 1.33.

4.5 Virtual Velocity Components

4.5.1 Resting Time

Resting times were represented by a rapidly decreasing power law function of τ^* . By using the parameters of Eq.(49) the results collapse to a single power law (Figure 4.6) of the form of Eq.(50) below

$$T_r^* = a_1 (\tau^* R_r^{1.33})^{a_2} \quad (50)$$

where a_1 and a_2 get the values of 3.36×10^{-16} and -9.59, respectively. The dimensionless resting time T_r^* is defined as

$$T_r^* = \frac{T_r}{\sqrt{\frac{d}{\left(\frac{\rho_s}{\rho_w} - 1\right) g}}} \quad (51)$$

The probability density functions (PDFs) of resting times showed an interesting dependence to the dimensionless shear stress and the relative roughness. The conclusions of the analysis of the PDFs is that for high transport conditions an exponential distribution can be used to model the PDFs of resting times. But for low transport conditions a Weibull or a Gamma distribution is more appropriate. The merit of using a Weibull or a Gamma distribution to model the PDFs of resting times has been pointed out by Witz (2015). Since the main goal of this study is related to mean values of resting time, the analysis of the PDFs of resting times is presented in the Appendix B.

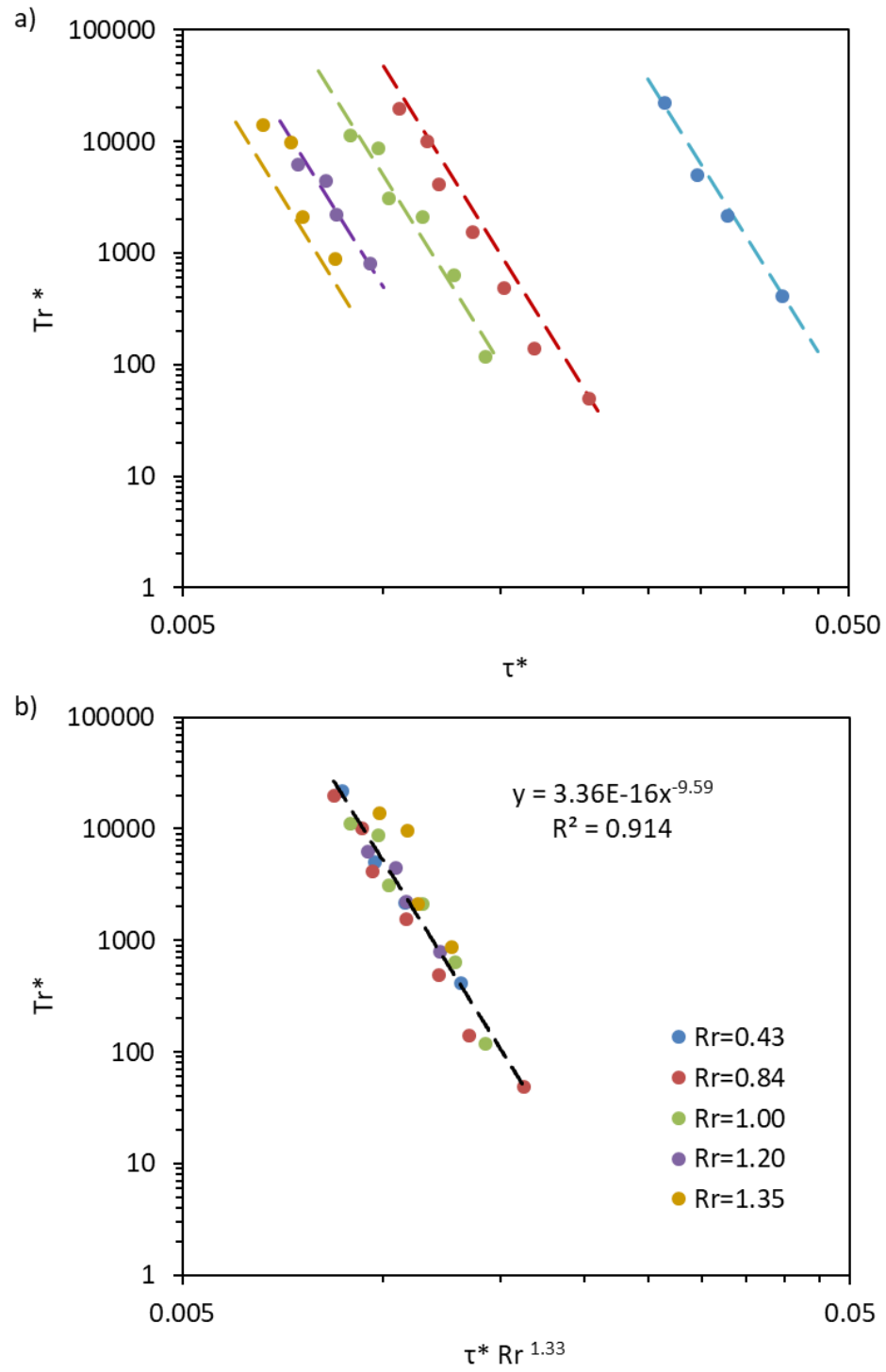


Figure 4.6 Dimensionless resting time as a function of a) τ^* , and b) $\tau^* Rr^{1.33}$.

4.5.2 Displacement Length

Dimensionless displacement length as it depends on each dimensionless shear stress and on the parameter from Eq.(49) are plotted in Figure 4.7. Same as with the resting time, the displacement length also collapses to a single power law when the parameter from Eq.(49) is used. The power law for the displacement length takes the form below

$$L^* = a_3 (\tau^* R_r^{1.33})^{a_4} \quad (52)$$

where a_3 and a_4 are constants that for the experiments of this study take the values of 6.3×10^7 and 3.51, respectively. The dimensionless displacement length was calculated as the displacement length divided with the diameter of the moving particle as follows:

$$L^* = \frac{L}{d} \quad (53)$$

4.5.3 Displacement Velocity

The displacement velocity equation, Eq.(12), developed by Cheng and Emadzadeh (2014) aligned with data from this study. For well-packed, fixed beds with spherical particles of uniform size (i.e. R_r is equal to 1), Cheng and Emadzadeh (2014) proposed values for c_1 , c_2 of Eq.(12) to be 11.1 and 1.0 respectively. In addition, the values of the constant n that they used throughout their study is 0.6.

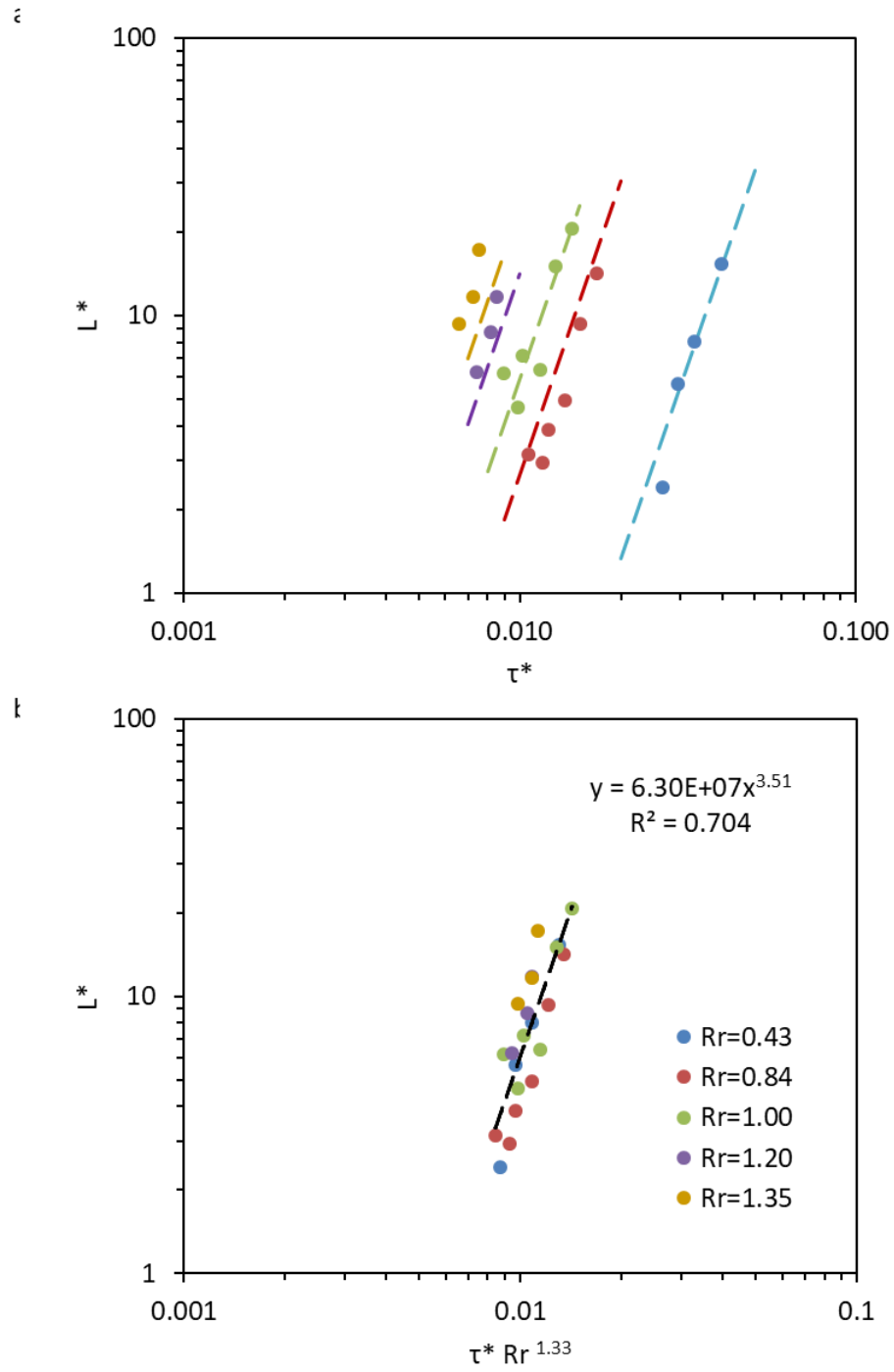


Figure 4.7 Dimensionless displacement length as a function of a) τ^* , and b) $\tau^* R_r^{1.33}$.

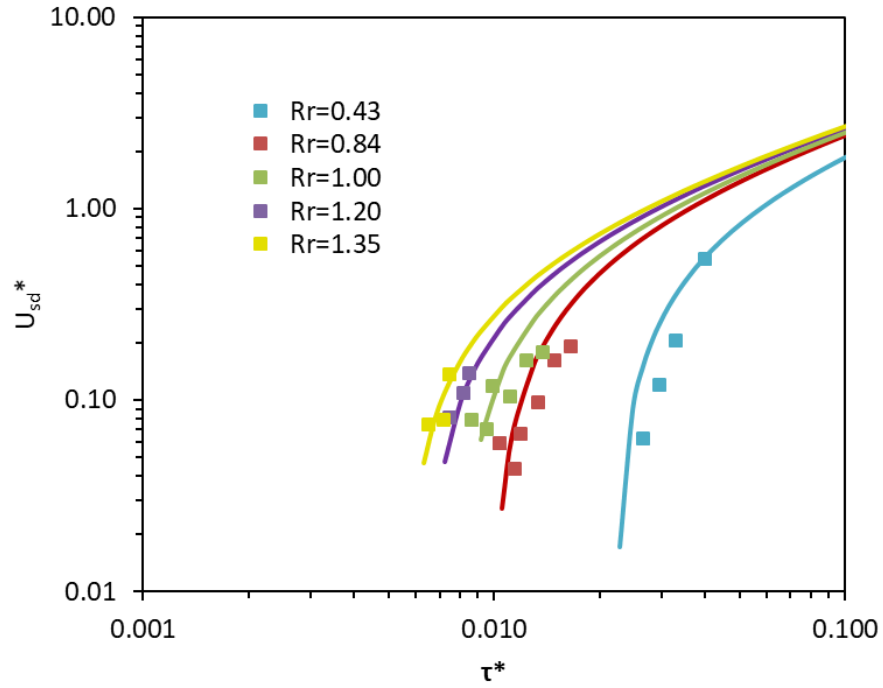


Figure 4.8 Plot of the study data with the computed lines from Eq.(12) by Cheng and Emadzadeh (2014) using the values they proposed for their constants in Eq.(12).

This value for n also collapsed with the data of this study. Data from this study are plotted in Figure 4.8 with the computed lines from Eq.(12) for different R_r values.

4.5.4 Virtual Velocity

In Figure 4.9, virtual velocity data from this study are plotted along with the calculated virtual velocities for different R_r values. Virtual velocity, U_{sv} , was calculated from the displacement length, L , the resting time, T_r , and the displacement time, T_d , as

defined in Eq.(1). The displacement length, L , and the resting time, T_r , were calculated from the Eq.(52) and Eq.(50) respectively. The displacement time, T_d , was calculated using the definition in Eq.(22), the calculated displacement length, L , and the calculated U_{sd} from the Eq.(12) developed by Cheng and Emadzadeh (2014). The values for the virtual velocity were normalized using the equation below:

$$U_{sv}^* = \frac{U_{sv}}{\sqrt{\left(\frac{\rho_s}{\rho_w} - 1\right)gd}} \quad (54)$$

Calculated and measured virtual velocities are compared in Figure 4.10. The coefficient of determination, R^2 , was calculated using the equation below:

$$R^2 = 1 - \frac{\sum \left[(U_{sv,exp} - U_{sv,calc})^2 \right]}{\sum \left[(U_{sv,exp} - \overline{U_{sv,exp}})^2 \right]} \quad (55)$$

where $U_{sv,exp}$ were the experimental data values for virtual velocity and $U_{sv,calc}$ were the calculated values for virtual velocity. The R^2 was found to be equal to 0.97, which indicates that the model equations fit really well the experimental values.

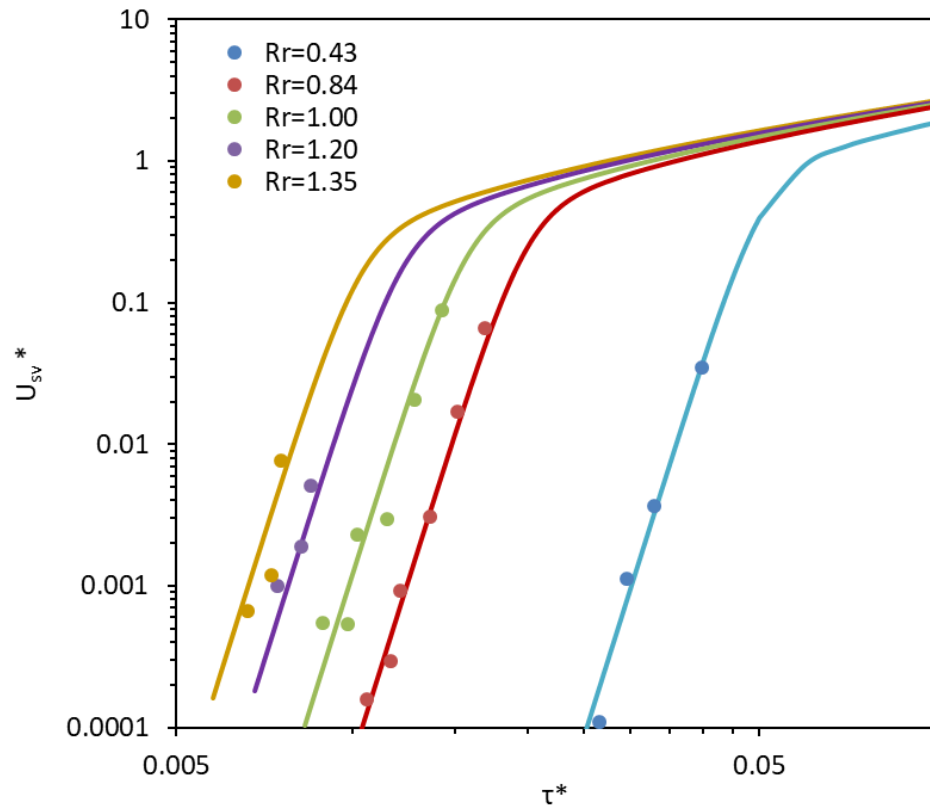


Figure 4.9 Virtual velocity data plotted along with the computed virtual velocity lines for different R_r values.

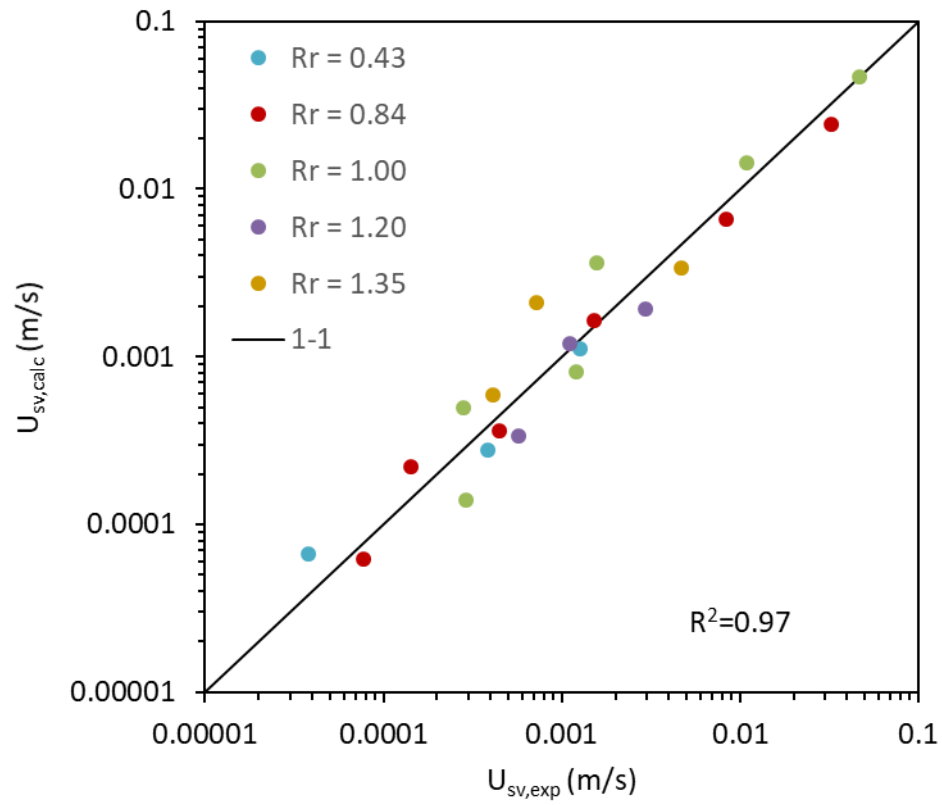


Figure 4.10 Comparison of the calculated and the measured virtual velocities.

5 CONCLUSIONS AND RECOMMENDATIONS

The virtual velocity of bedload particles was investigated via laboratory flume experiments using marbles of different sizes transported on top of a well-packed marble bed for a wide range of flow conditions. In these experiments, the trajectories of the moving particles were captured using a camera and tracked using an open source particle tracking code.

The motivation in defining virtual velocity is to enhance the predictions of bedload transport rates. The bedload transport rates can be calculated with a Lagrangian approach by multiplying the virtual velocity of particles with the number of particles that are able to be mobilized per unit area and the representative mass per particle. Dividing sediment particles in different size fractions further increases the accuracy of the prediction for the total bedload rate (total bedload rate in this case is calculated as the sum of the bedload rates predicted for each different size fraction). If the sediment is divided in different size fractions the effects of relative roughness on the virtual velocities of each size fraction needs to be accounted in the calculations.

Other studies have also focused on computing virtual velocity via field or laboratory experiments. The limitations of the field studies were the lack of detailed measurements of intermittent trajectories. They only record the initial and final location and then calculate virtual velocity as the total distance over the total time. Furthermore, the field conditions are not controlled, which introduces uncertainties in the independent variables. This results in discrepancies in virtual velocity equations developed by different studies. In addition, no laboratory study for gravel-size particles was found in the literature that examined the virtual velocity of gravel-size particles for a wide range of particle sizes and flow conditions ranging from incipient motion to high transport. This study provides unique data that fill this research gap in the literature.

The contribution of this study includes the development of new modeling equations to calculate virtual velocity. It was shown that the use of the ratio of dimensionless bed

shear to critical shear stress collapses the data for the displacement length and the resting time. The critical shear stress was calculated as a power law of relative roughness (which is widely encountered in the literature). The data were used to develop simple practical equations pertaining to moderate slope gravel-bed streams, that predict the mean displacement length and resting time of particles. To the author's knowledge, no equation has been developed before in the literature to predict resting times. For the displacement velocity, an equation from literature was found to perform well and there was no need to develop a new equation. These equations were combined to predict the virtual velocity of particles. A novelty of this study is that it models each component of virtual velocity separately (displacement length, resting time and displacement velocity), and combines them to predict virtual velocity, in contrast to the more common practice that is to use only one equation to predict virtual velocity directly. It is believed by the author that calculating virtual velocity by modeling each subcomponent separately is a more fundamental approach that increases the accuracy of the virtual velocity prediction.

This study suggests that the ratio of dimensionless shear stress to critical shear stress can be used to model the virtual velocity components in moderate slope gravel-bed rivers. The most important differences of the natural streams to the laboratory experiments of this study is that natural river beds are not well-packed and naturally worn grains are not perfect spheres. These differences affect the resistance forces by increasing the angle of repose and the mobilizing forces by affecting both the drag coefficient and protrusion. Due to these differences, the equations developed in this study are not directly applicable to predict virtual velocity in natural streams. The exponent in the power law relationship between the critical shear stress and the relative roughness that is used in this study relates to marbles. Future research is needed to investigate the use of a power applicable for natural gravel to predict the displacement length and resting time of natural gravel via the equations developed in this study. If this is accomplished, these equations can be combined with an equation of displacement velocity of natural gravel which is well established in the literature to predict virtual velocity of natural gravel.

REFERENCES

- Ballio, F., Pokrajac, D., Radice, A., and Hosseini Sadabadi, S. A. (2018). “Lagrangian and Eulerian Description of Bed Load Transport.” *Journal of Geophysical Research: Earth Surface*, 123, 384–408.
- Ballio, F., Radice, A., Fathel, S. L., and Furbish, D. J. (2019). “Experimental Censorship of Bed Load Particle Motions and Bias Correction of the Associated Frequency Distributions.” *Journal of Geophysical Research: Earth Surface*, 124, 116–136.
- Bettess, R. (1984). “Initiation of Sediment Transport in Gravel Streams.” *Proceedings - Institution of Civil Engineers, Part 2*, 77, 79–88.
- Cantwell, B. J. (1981). “Organized Motion in Turbulent Flow.” *Annual review of fluid mechanics*, 13, 457–515.
- Celik, A. O., Diplas, P., and Dancey, C. L. (2013). “Instantaneous turbulent forces and impulse on a rough bed: Implications for initiation of bed material movement.” *Water Resources Research*, 49(4), 2213–2227.
- Cheng, N. S., and Chua, L. H. C. (2005). “Comparisons of sidewall correction of bed shear stress in open-channel flows.” *Journal of Hydraulic Engineering*, 131(7), 605–609.
- Cheng, N. S., and Emadzadeh, A. (2014). “Average velocity of solitary coarse grain in flows over smooth and rough beds.” *Journal of Hydraulic Engineering*, 140(6), 1–12.
- Church, M., and Hassan, M. A. (1992). “Size and distance of travel of unconstrained clasts on a streambed.” *Water Resources Research*, 28(1), 299–303.
- Clauser, F. H. (1956). “The Turbulent Boundary Layer.” *Advances in Applied Mechanics*, Academic Press INC., New York, 1–51.
- Diplas, P. (1987). “Bedload Transport in Gravel-Bed Streams.” *Journal of Hydraulic Engineering*, 113, 277–292.
- Einstein, H. A. (1950). “The Bed-Load Function for Sediment Transportation in Open Channel Flows.” *Technical Bulletin No. 1026, U.S. Department of Agriculture, Washington D.C.*
- Fathel, S. L., Furbish, D. J., and Schmeeckle, M. W. (2015). “Experimental evidence of statistical ensemble behavior in bed load sediment transport.” *Journal of Geophysical Research: Earth Surface*, 120, 2298–2317.

- Ferguson, R. I., Bloomer, D. J., Hoey, T. B., and Werritty, A. (2002). "Mobility of river tracer pebbles over different timescales." *Water Resources Research*, 38(5), 3-1-3-8.
- Ferguson, R. I., and Wathen, S. J. (1998). "Tracer-pebble movement along a concave river profile: Virtual velocity in relation to grain size and shear stress." *Water Resources Research*, 34(8), 2031-2038.
- Fraccarollo, L., and Hassan, M. A. (2019). "Einstein conjecture and resting-Time statistics in the bed-load transport of monodispersed particles." *Journal of Fluid Mechanics*, 876, 1077-1089.
- García, C., Cantero, M., Niño, Y., and García, M. (2005). "Doppler Velocimeters." *Journal of Hydraulic Engineering*, 131(12), 1062-1073.
- García, M. (2008). *Sedimentation Engineering: Processes, Measurements, Modeling, and Practice*. American Society of Civil Engineers.
- Haschenburger, J. K., and Church, M. (1998). "Bed material transport estimated from the virtual velocity of sediment." *Earth Surface Processes and Landforms*, 23(9), 791-808.
- Haschenburger, J. K., and Wilcock, P. R. (2003). "Partial transport in a natural gravel bed channel." *Water Resources Research*, 39(1), 1-9.
- Heyman, J. (2019). "TracTrac: A fast multi-object tracking algorithm for motion estimation." *Computers and Geosciences*, 128, 11-18.
- Hunt, A. G., and Papanicolaou, A. N. (2003). "Tests of predicted downstream transport of clasts in turbulent flow." *Advances in Water Resources*, 26, 1205-1211.
- Kironoto, B. A., and Graf, W. H. (1995). "Turbulence characteristics in rough uniform open-channel flow." *Proceedings of the Institution of Civil Engineers: Water, Maritime and Energy*, 106, 333-344.
- Klösch, M., and Habersack, H. (2018). "Deriving formulas for an unsteady virtual velocity of bedload tracers." *Earth Surface Processes and Landforms*, 43, 1529-1541.
- Knapp, D. (2002). "Applications of particle velocity to bedload motion." Washington State University.
- Lajeunesse, E., Malverti, L., and Charru, F. (2010). "Bed load transport in turbulent flow

- at the grain scale: Experiments and modeling.” *Journal of Geophysical Research*, 115.
- Mao, L., Picco, L., Lenzi, M. A., and Surian, N. (2017). “Bed material transport estimate in large gravel-bed rivers using the virtual velocity approach.” *Earth Surface Processes and Landforms*, 42(4), 595–611.
- Meyer-Peter, E., and Müller, R. (1948). “Formulas for Bed-Load Transport.” *Proceedings of the 2nd Meeting of the International Association of Hydraulic Research*, International Association of Hydraulic Research, Stockholm, 39–64.
- Milan, D. J. (2013). “Virtual velocity of tracers in a gravel-bed river using size-based competence duration.” *Geomorphology*, 198, 107–114.
- Niño, Y., and García, M. (1998). “Experiments on Saltation of Sand in Water.” *Journal of Hydraulic Engineering*, 124(10), 1014–1025.
- Papanicolaou, A., Douglas, K., and Kyle, S. (2002a). “Bedload Predictions by Using the Concept of Particle Velocity: Applications.” *Hydraulic Measurements and Experimental Methods 2002*.
- Papanicolaou, A. N., Bdour, A., and Wicklein, E. (2004). “One-dimensional hydrodynamic/sediment transport model applicable to steep mountain streams.” *Journal of Hydraulic Research*, 42(4), 357–375.
- Papanicolaou, A. N., Diplas, P., Evaggelopoulos, N., and Fotopoulos, S. (2002b). “Stochastic incipient motion criterion for spheres under various bed packing conditions.” *Journal of Hydraulic Engineering*, 128, 369–380.
- Papanicolaou, A. N., Kramer, C. M., Tsakiris, A. G., Stoesser, T., Bomminayuni, S., and Chen, Z. (2012). “Effects of a fully submerged boulder within a boulder array on the mean and turbulent flow fields: Implications to bedload transport.” *Acta Geophysica*, 60(6), 1502–1546.
- Parker, G. (1990). “Surface-based bedload transport relation for gravel rivers.” *Journal of Hydraulic Research*, 28(4), 417–436.
- Parsons, A. J., Cooper, J., Wainwright, J., and Sekiguchi, T. (2018). “Virtual velocity of sand transport in water.” *Earth Surface Processes and Landforms*, 43, 755–761.
- Shields, A. (1936). *Anwendung der Aenlichkeitsmechanik und der Turbulenzforschung auf*

die Geschiebepbewegung. Mitteilungen der Preussischen Versuchsanstalt für Wasserbau und Schiffbau, Berlin, Germany.

- Vanoni, V. A. (2006). "Sedimentation Engineering." American Society of Civil Engineers, Reston, VA.
- Vázquez-Tarrió, D., Recking, A., Liébault, F., Tal, M., and Menéndez-Duarte, R. (2019). "Particle transport in gravel-bed rivers: Revisiting passive tracer data." *Earth Surface Processes and Landforms*, 44, 112–128.
- Wilcock, P. R., and McArdell, B. W. (1997). "Partial transport of a sand/gravel sediment." *Water Resources Research*, 33(1), 235–245.
- Witz, M. J. (2015). "Mechanics of Particle Entrainment in Turbulent Open-Channel Flows." University of Aberdeen.
- Wong, M., Parker, G., DeVries, P., Brown, T. M., and Burges, S. J. (2007). "Experiments on dispersion of tracer stones under lower-regime plane-bed equilibrium bed load transport." *Water Resources Research*, 43, 1–23.
- Wu, F. C., and Yang, K. H. (2004). "A stochastic partial transport model for mixed-size sediment: Application to assessment of fractional mobility." *Water Resources Research*, 40.
- Wu, W., Wang, S. S. Y., and Jia, Y. (2000). "Nonuniform sediment transport in alluvial rivers." *Journal of Hydraulic Research*, 38(6), 427–434.
- Wu, Z., Furbish, D., and Foufoula-Georgiou, E. (2020). "Generalization of Hop Distance-Time Scaling and Particle Velocity Distributions via a Two-Regime Formalism of Bedload Particle Motions." *Water Resources Research*, 56(1), 1–14.

APPENDICES

A AVERAGING METHODS FOR DISPLACEMENT VELOCITIES

Ballio et al. (2018) pointed out that the displacement velocity calculated by the mean displacement and mean displacement time is different from the mean of all the displacement velocities calculated for each intermittent trajectory separately, as described by the inequality below

$$\overline{L}/\overline{T_d} \neq \overline{(L/T_d)} \quad (56)$$

This inequality (shown in Figure A.1) is a general property of averaged quantities. The difference between the two averages is due to the fact that the displacement length is typically not linearly correlated with the corresponding displacement time as shown by Fathel et al. (2015). The left hand side of the inequality in Eq.(56) is the proper way to calculate the displacement velocity so it can be used to predict virtual velocity.

The correlation between displacement length and displacement time is clear and evident in all of the datasets of this study. Just for demonstration, this correlation is presented for one of the conditions tested in this study in Figure A.2. The power of T_d^2 for the lower displacement lengths shows that for the smaller displacements the acceleration and deceleration periods are a significant percentage of the T_d . For higher T_d the U_{sd} increases and thus L relationship with T_d is non-linear. But, when a certain L value is exceeded, the U_{sd} reaches a steady state, and the deceleration and acceleration periods become less important for the U_{sd} value since they are a small percentage of the T_d and. Thus, L tends to become a linear function of T_d . The relationship of L with T_d^2 for lower L values and with T_d for higher L values have been observed also by Wu et al. (2020).

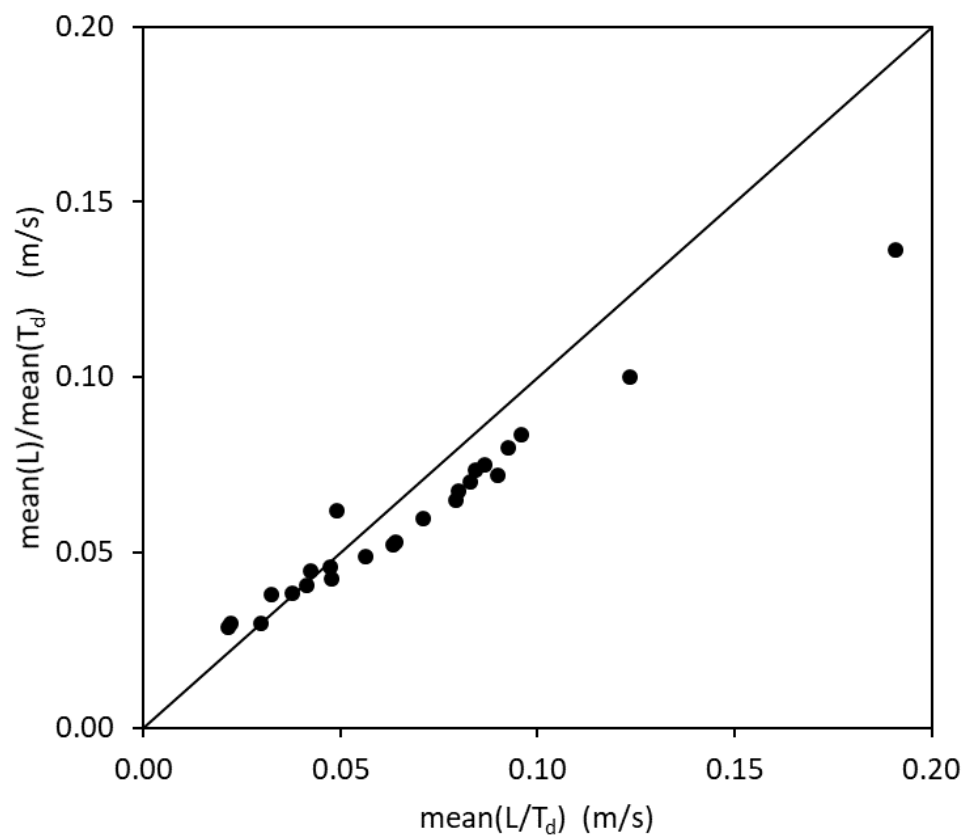


Figure A.1 Differences in averaging method for displacement velocity.

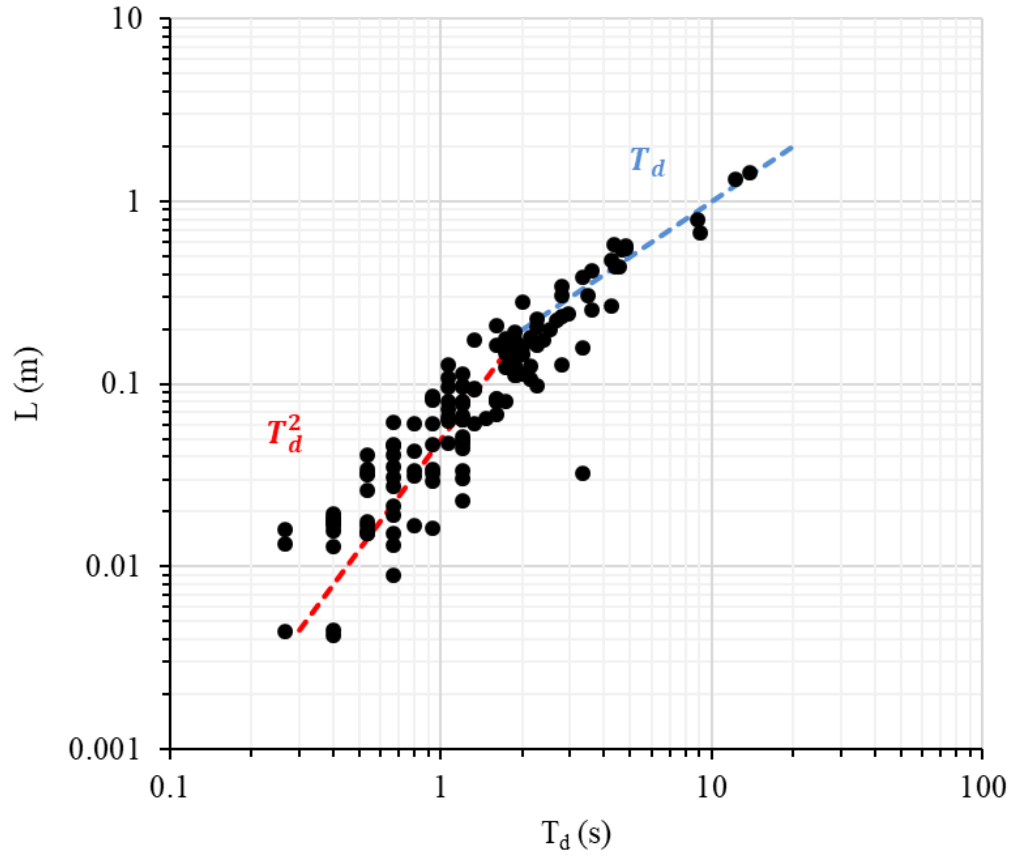


Figure A.2 Non-linear relationship between displacement length and displacement time for the smaller displacements for the experiment with Rr equal to 0.84 and τ^* equal to 0.0152.

B STATISTICS OF RESTING TIMES

For each condition the number of resting time data collected was between 60 and 250. This allowed to plot probability density functions (PDFs) for each condition. The analysis of the normalized PDFs showed an interesting pattern. While for high transport the resting times seem to be exponentially distributed, for the low transport regime the exponential distribution assumption is not performing well.

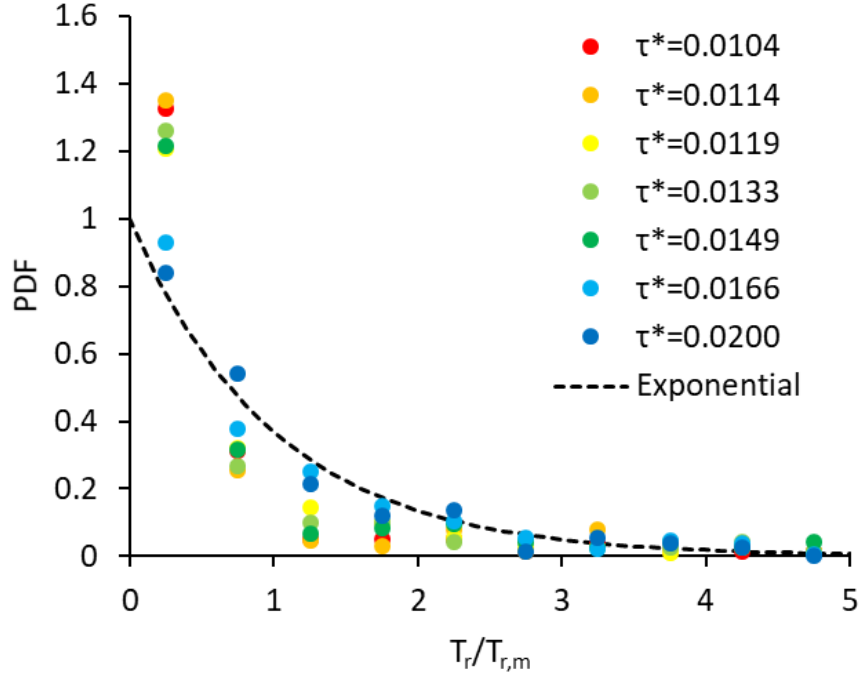


Figure B.1 Normalized probability density functions of resting times corresponding to different transport stages for Rr equal to 0.84.

Witz (2015) has proposed that either a Weibull distribution or a Gamma distribution may be more suited to describe the PDFs of resting times. These distributions can capture the shape of the PDFs more accurately than the Exponential distribution, by adjusting their shape parameter. This result is not only verified by looking at the data of this study in Figure B.1, but it appears there is a relationship between τ^* and the value of the shape parameter of the distribution. The Eq.(57) and the Eq.(58) show the PDFs of the Weibull and the Gamma distribution respectively

$$PDF_{Weib} = \frac{k}{\lambda} \left(\frac{x}{\lambda}\right)^{k-1} e^{(-x/\lambda)^k} \quad (57)$$

$$PDF_{Gam} = \frac{\beta^\alpha}{\Gamma(\alpha)} x^{\alpha-1} e^{-\beta x} \quad (58)$$

where k and α are the shape parameters of the Weibull and Gamma distribution respectively. The λ is the scale parameter of the Weibull distribution, the β is the inverse of the scale parameter of the Gamma distribution and the Γ is the gamma function. The x is the random variable (here is the resting time normalized with the mean resting time).

The Eq.(57) and the Eq.(58) are fitted to the data for all tests and the shape parameters are presented in Table B.1. Examining Table B.1 and Figure B.1 it is obvious that the shape parameters are positively correlated with τ^* for all values of Rr . An observation made using these data was that the distribution is related to the transport stage. In the high transport regime that is close to general motion, the distribution can be described by an Exponential distribution (i.e. Weibull with k parameter equal to 1). As the resting time increases, the shape parameter k decreases approaching a value of 0.5 as it approaches the threshold for motion condition. The same behavior was observed for the shape parameter α for the Gamma distribution. Figure B.2 showed this trend by plotting the shape parameters as a function of dimensionless resting times. The data by Witz (2015) are

included in the Figure B.2 as a comparison. The uniqueness of the data of this study was that they cover a wide range of transport stages from very low to very high transport, and the trend in the shape parameters can be observed. The data by Witz (2015) were not capable to show this trend.

Table B.1 Values for the shape parameters for the Weibull and the Gamma distribution for all the conditions of this study.

Rr	τ^*	k	a
0.43	0.0265	0.53	0.40
0.43	0.0296	0.63	0.51
0.43	0.0329	0.69	0.58
0.43	0.0398	0.75	0.66
0.84	0.0104	0.56	0.42
0.84	0.0114	0.50	0.37
0.84	0.0119	0.56	0.42
0.84	0.0133	0.63	0.51
0.84	0.0149	0.73	0.66
0.84	0.0166	0.97	1.02
0.84	0.0200	1.16	1.49

Rr	τ^*	k	a
1.00	0.0086	0.51	0.37
1.00	0.0095	0.49	0.36
1.00	0.0099	0.55	0.42
1.00	0.0111	0.57	0.44
1.00	0.0124	0.67	0.57
1.00	0.0138	0.83	0.80
1.20	0.0074	0.52	0.39
1.20	0.0082	0.50	0.36
1.20	0.0085	0.48	0.34
1.20	0.0096	0.59	0.47
1.33	0.0065	0.38	0.26
1.33	0.0072	0.35	0.23
1.35	0.0074	0.49	0.35
1.35	0.0084	0.50	0.36

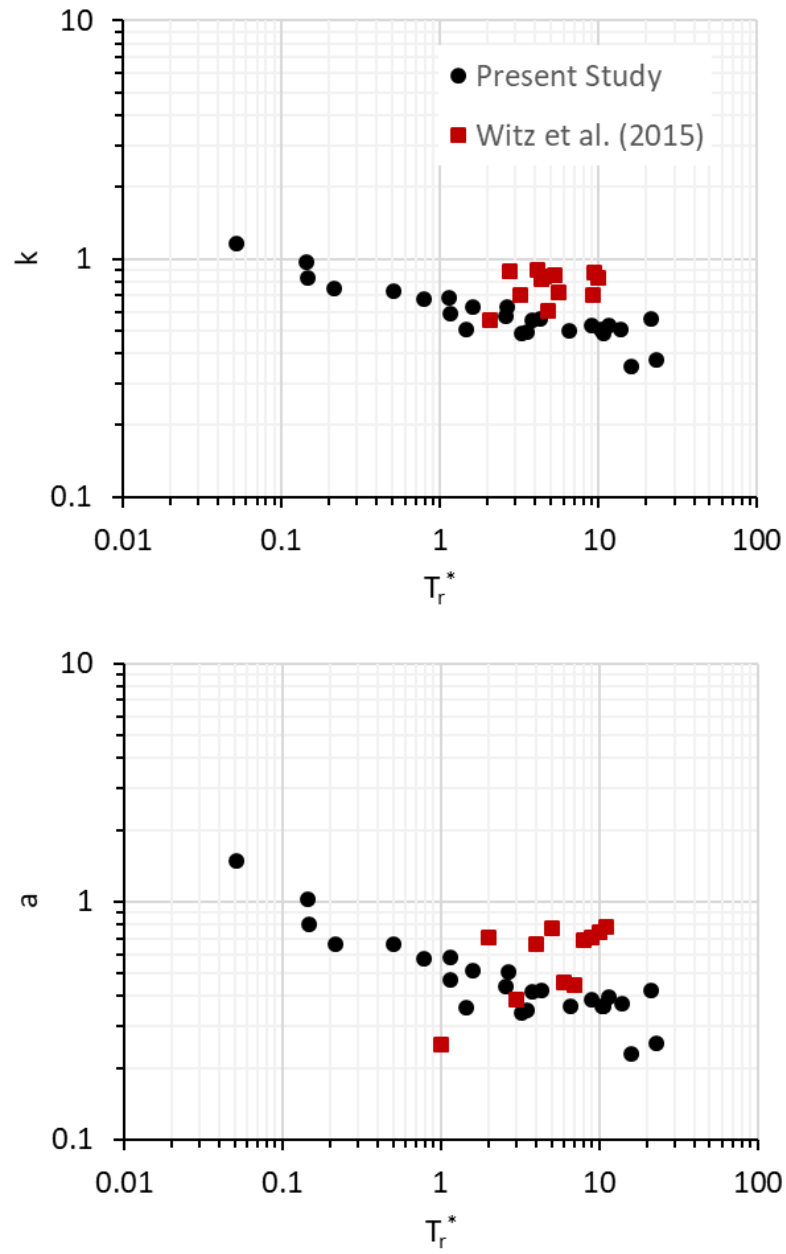


Figure B.2 Shape parameter for Weibull and Gamma distributions as a function of dimensionless resting time.

VITA

Theodoros Kyriakopoulos was born and raised in Athens, Greece. Theodoros studied Civil Engineering at the University of Patras, in Greece. After graduation, he was enrolled to the interdepartmental Masters Program “Design and Construction of Underground Works” at the National Technical University of Athens (NTUA), in Greece. After graduating from the NTUA, he was awarded the Chancellor’s Top Off Fellowship from The University of Tennessee, he started working as a Graduate Research Assistant and he was enrolled in the Environmental Engineering Masters program with concentration in Water Resources Engineering. He graduated in August, 2020.